Geochemistry Geophysics Geosystems G3

Article
Volume 14, Number 7
19 July 2013
doi: 10.1002/ggge.20173
ISSN: 1525-2027

Published by AGU and the Geochemical Society

Active deformation in old oceanic lithosphere and significance for earthquake hazard: Seismic imaging of the Coral Patch Ridge area and neighboring abyssal plains (SW Iberian Margin)

Sara Martínez-Loriente, Eulàlia Gràcia, Rafael Bartolome, and Valentí Sallarès
Barcelona Center for Subsurface Imaging, Institut de Ciències del Mar, CSIC, Barcelona, Spain (smartinez@cmima.csic.es)

Christopher Connors
Department of Geology, Washington and Lee University, Lexington, Virginia, USA

Hector Perea and Claudio Lo Iacono
Barcelona Center for Subsurface Imaging, Institut de Ciències del Mar, CSIC, Barcelona, Spain

Dirk Klaeschen
IFM-GEOMAR, Dynamik des Ozeanbodens, Wischhofstrasse, Kiel, Germany

Pedro Terrinha
Instituto Português do Mar e da Atmosfera, Rua C—Aeroporto de Lisboa, Lisboa, Portugal

Juan José Dañobeitia
Unidad de Tecnología Marina, CSIC, Barcelona, Spain

Nevio Zitellini
Sezione Geologia Marina, Istituto Scienze Marine, CNR, Bologna, Italy

[1] Recently acquired high-resolution multichannel seismic profiles together with bathymetric and sub-bottom profiler data from the external part of the Gulf of Cadiz (Iberia-Africa plate boundary) reveal active deformation involving old (Mesozoic) oceanic lithosphere. This area is located 180 km offshore the SW Iberian Peninsula and embraces the prominent NE-SW trending Coral Patch Ridge, and part of the surrounding deep Horseshoe and Seine abyssal plains. E-W trending dextral strike-slip faults showing surface deformation of flower-like structures predominate in the Horseshoe Abyssal Plain, whereas NE-SW trending compressive structures prevail in the Coral Patch Ridge and Seine Hills. Although the Coral Patch Ridge region is characterized by subdued seismic activity, the area is not free from seismic hazard. Most of the newly mapped faults correspond to active blind thrusts and strike-slip faults that are able to generate large magnitude earthquakes (*Mw* 7.2–8.4). This may represent a significant earthquake and tsunami hazard that has been overlooked so far.

Components: 13,212 words, 10 figures, 1 table.

Keywords: multichannel seismics; fault-bend folds; blind thrusts; strike-slip faults; seismic hazard assessment; Iberia-Africa boundary.

Index Terms: 3025: Marine Geology and Geophysics: Marine seismics; 3045: Marine Geology and Geophysics: Seafloor morphology, geology, and geophysics; 8104: Tectonophysics: Continental margins: convergent; 7230: Seismology: Seismicity and Tectonics; 9325: Geographic Location: Atlantic Ocean.

Received 29 March 2013; **Revised** 10 May 2013; **Accepted** 10 May 2013; **Published** 19 July 2013.

Martínez-Loriente, S., E. Gràcia, R. Bartolome, V. Sallarès, C. Connors, H. Perea, C. Lo Iacono, D. Klaeschen, P. Terrinha, J. J. Dañobeitia, and N. Zitellini (2013), Active deformation in old oceanic lithosphere and significance for earthquake hazard: Seismic imaging of the Coral Patch Ridge area and neighboring abyssal plains (SW Iberian Margin), *Geochem. Geophys. Geosyst., 14*, 2206–2231, doi:10.1002/ggge.20173.

1. Introduction

[2] Active deformation involving old (Mesozoic) oceanic lithosphere is relatively uncommon [e.g., *Weissel et al*., 1980; *Bull and Scrutton*, 1990, 1992] and one of the few examples corresponds to the external part of the Gulf of Cadiz, offshore SW Iberia [e.g., *Sartori et al*., 1994; *Rovere et al*., 2004]. This area, which is interpreted to be underlain by Jurassic-Cretaceous age oceanic lithosphere on the basis of refraction and wide-angle reflection seismics (WAS), magnetic data, and kinematic reconstructions [e.g., *Ryan et al*., 1973; *Purdy*, 1975; *Contrucci et al*., 2004; *Rovere et al*., 2004; *Schettino and Turco*, 2009; *Martínez-Loriente et al*., 2011; *Sallarès et al*., 2011, 2013], undergoes quaternary deformation consequence of the NW-SE trending Eurasia-Africa plate convergence (3.8–5.6 mm/yr) [*Nocquet and Calais*, 2004; *DeMets et al*., 2010]. Seismic activity is mainly of moderate magnitude ($Mw < 6.0$), although large magnitude destructive earthquakes, such as the 1755 Lisbon Earthquake and Tsunami nucleated in the external part of the Gulf of Cadiz (Figure 1).

[3] During the last two decades, numerous geological and geophysical surveys have been carried out in the region seeking faults that may be potential sources of large magnitude earthquakes [e.g., *Sartori et al*., 1994; *Tortella et al*., 1997; *Hayward et al*., 1999; *Gutscher et al*., 2002; *Gràcia et al*., 2003a, 2003b; *Terrinha et al*., 2003, 2009; *Zitellini et al*., 2001, 2004, 2009; *Bartolome et al*., 2012]. One of the outstanding results has been the recognition of the SWIM Fault Zone (SFZ), a 600 km long dextral strike-slip deformation zone connecting the Gorringe Bank with the Moroccan shelf [*Zitellini et al*., 2009] (Figure 1). The present work focuses on the area of the external part of the Gulf of Cadiz located south of the SFZ, which comprises the Coral Patch Ridge and part of the neighboring Horseshoe and Seine abyssal plains. The tectonic structures of this area have been considered as inactive mainly due to (1) the lack of instrumental seismicity associated with them [*Zitellini et al*., 2009], and (2) the low resolution of pre-existing multichannel seismic (MCS) profiles, where deformation of Quaternary units could not be recognized [e.g., *Sartori et al*., 1994; *Tortella et al*., 1997] (Figures 1 and 2).

[4] The aim of this study is to characterize the pattern and timing of the deformation of the tectonic structures located in the Coral Patch Ridge region as well as Horseshoe and Seine abyssal plains, floored by Mesozoic oceanic lithosphere (Figure 2). Using acoustic and multiscale seismic data, we demonstrate that although there is little seismicity associated with these tectonic structures, they accommodate part of the present-day Eurasian-African plate convergence, and are therefore active. Finally, we evaluate the seismic potential of the most relevant active structures on the basis of their fault parameters (i.e., geometry, kinematics, maximum magnitude). Our findings demonstrate that the newly mapped structures represent a significant earthquake and tsunami hazard for the South Iberian and North African coasts that has not been accounted for to date.

2. Geological Setting of the External Part of the Gulf of Cadiz

[5] The morphology and tectonic structure of the external part of the Gulf of Cadiz results from the complex geodynamic history undergone by the region since the opening of the Western Tethyan, Central- and North-Atlantic oceans during the Mesozoic [e.g., *Tucholke et al*., 2007; *Schettino and Turco*, 2009], combined with the changes in location and kinematics of the Eurasian-African plate boundary [*Srivastava et al*., 1990]. Consequently, the nature of the basement in this area has been the subject of an enduring debate [e.g., *Purdy*, 1975; *Sartori et al*., 1994; *Tortella et al*., 1997; *Hayward et al*., 1999; *Jiménez-Munt et al*., 2010]. Recently acquired WAS profiles suggest the presence of oceanic crust of Jurassic age in the central Gulf

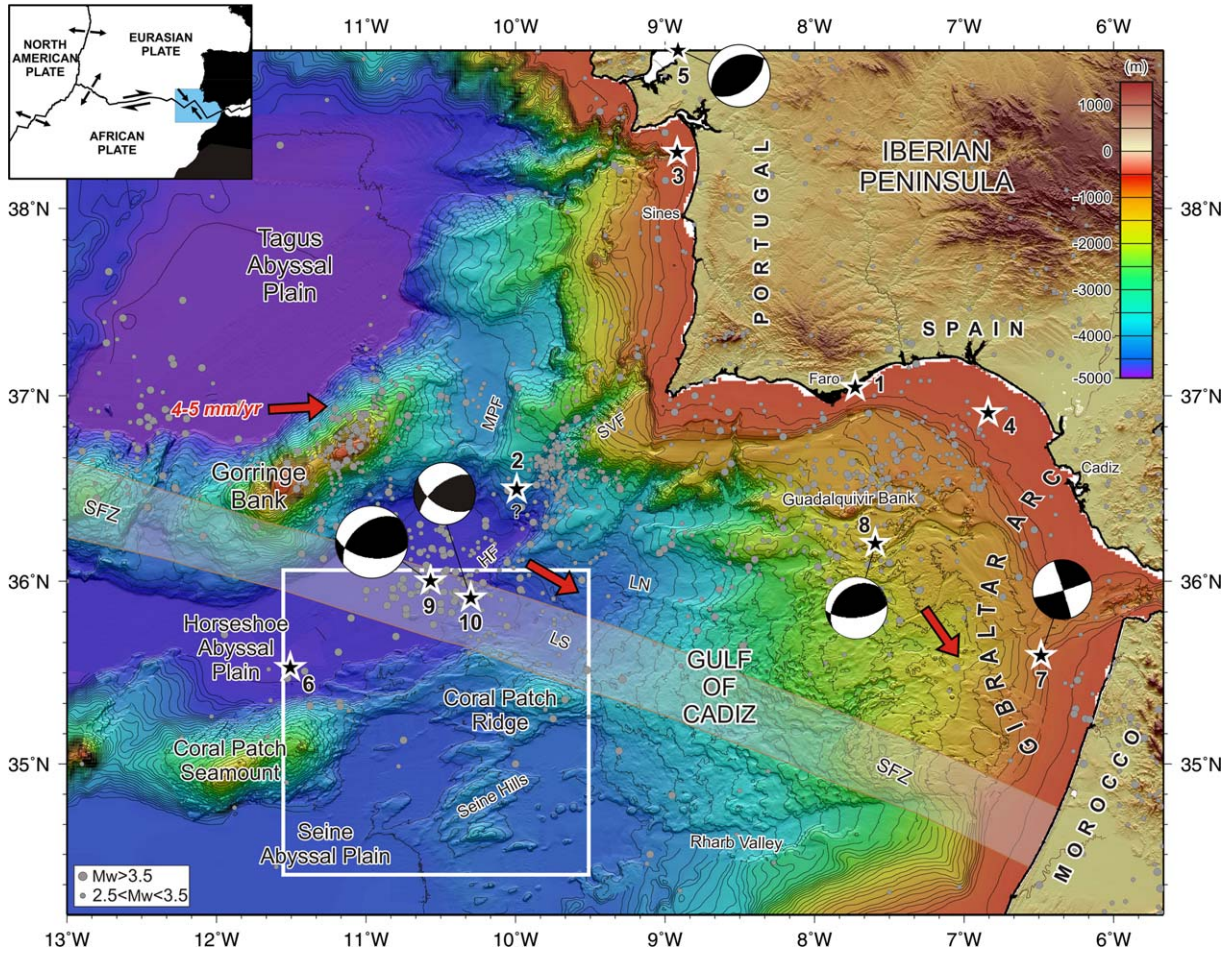

Figure 1. Regional topographic and bathymetric map of the southwest Iberian margin constructed from digital grids (~90 m grid size) released by SRTM-3 and the ESF EuroMargins SWIM multibeam compilation [*Zitellini et al*, 2009]. Seismicity from the Instituto Geográfico Nacional catalogue for the period between 1965 and 2012 is depicted [*I.G.N.*, 2012]. Small gray dots are epicenters of earthquakes for $2.5 < M_w < 3.5$, and large gray dots for earthquakes of $M_w > 3.5$. Black stars correspond to epicenters of historical and instrumental earthquakes of $M_w \geq 6.0$ that occurred in the SW Iberian margin, whose fault plane solutions are depicted. 1: Tavira Earthquake, 27 December 1722, estimated M_w 6.5 [*Baptista and Miranda*, 2009]; 2: Proposed epicenter location for the Lisbon Earthquake (see text for details), 1 November 1755, estimated M_w 8.5 [*Buforn et al*., 2004]; 3: Setubal Earthquake, 11 November 1858, estimated M_w 7.1 [*Martínez-Solares*, 2003]; 4: 1883, estimated M_w 6.1, 5: Benavente Earthquake, 23 April 1909, M_w 6.0 [*Mezcua et al*., 2004]; 6: Horseshoe Earthquake, 7 November 1915, M_w 6.2 [IGN Catalogue]; 7: 5 December 1960, M_w 6.2 [*Buforn et al*., 2004]; 8: Guadalquivir Bank Earthquake, 15 March 1964, M_w 6.6 [*Stich et al*., 2005]; 9: Horseshoe Earthquake, 28 February 1969, M_w 7.9–8.0 [*Fukao*, 1973]; 10: HF Earthquake, 12 February 2007, M_w 6.0 [*Stich et al*., 2007]. Red arrows show the direction of convergence between the Eurasian and African plates from the NUVEL1 model [*Argus et al*., 1989]. The box outlined in white depicts the study area presented in Figure 2. HF: Horseshoe Fault [e.g., *Gràcia et al*., 2003a]; LN: Lineament North and LS: Lineament South [e.g., *Bartolome et al*., 2012]; MPF: Marquês de Pombal Fault [e.g., *Gràcia et al*., 2003a; *Terrinha et al*., 2003]; SVF: São Vicente Canyon Fault [e.g., *Gràcia et al*., 2003a]; SFZ gray band: SWIM Fault Zone [*Zitellini et al.*, 2009]. Inset: Plate tectonic setting of the southwest Iberian margin at the boundary between the Eurasian and African Plates. The blue rectangle corresponds to the area depicted in Figure 1.

of Cadiz [*Sallarès et al*., 2011], Coral Patch Ridge [*Martínez-Loriente et al*., 2011] and Seine Abyssal Plain [*Contrucci et al*., 2004; *Martínez-Loriente et al*., 2011], and of serpentinized mantle of Early Cretaceous age in the Gorringe Bank and under the sedimentary sequence infilling the southeastern Tagus and northern Horseshoe abyssal plains [*Sallarès et al*., 2013].

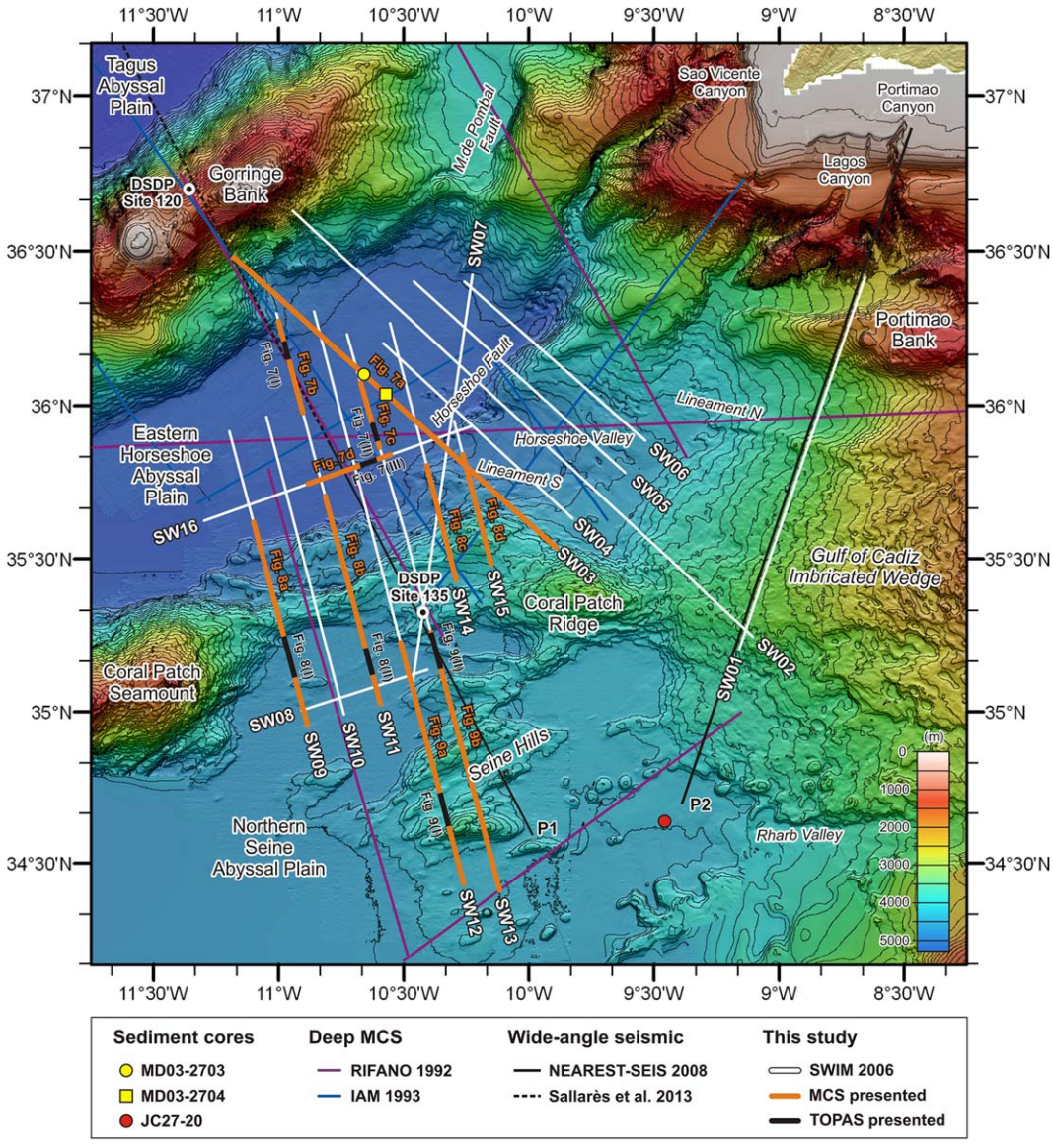

Figure 2. Color shaded-relief bathymetric map of the external part of the Gulf of Cadiz surveyed during the SWIM 2006 cruise. Contour interval is 50 m. Main morphostructural features are identified. The multichannel seismic reflection (MCS) profiles from the SWIM 2006 cruise presented in this study are depicted as thick orange lines, whereas TOPAS profiles are indicated by black thick lines. Deep MCS reflection (RIFANO 1992 and IAM 1993) [*Sartori et al*., 1994*; Tortella et al*., 1997] and wide-angle seismic (WAS) profiles (P1 and P2 from NEAREST-SEIS 2008) [*Martínez-Loriente et al*., 2011*; Sallarès et al*., 2011, 2013] used for this study are located. The portion of the WAS profile P1 presented in *Sallarès et al*. [2013] is depicted by a black dashed line. DSDP Sites 120 and 135 and sediment cores MD03-2703, MD03-2704, and JC27-20 are also located.

[6] The external part of the Gulf of Cadiz is characterized by a moderate magnitude seismicity mainly located between the Gorringe and Guadalquivir banks, and north of the SFZ [e.g., *Stich et al*., 2005]. This structure, interpreted as the present-day plate boundary between Africa and Eurasia, would act as a limit between the seismic and aseismic zones of the SW Iberian margin [e.g., *Zitellini et al*., 2009] (Figure 1). This region is also the source of large historical and instrumental earthquakes, such as the historical 1755 Lisbon Earthquake and Tsunami (estimated $Mw \geq 8.5$), the instrumental 1969 Horseshoe Earthquake (Mw 7.0–8.0) or, more recently, the 2007 Horseshoe

Fault (HF) Earthquake ($Mw = 6.0$) [*Fukao*, 1973; *Johnston*, 1996; *Baptista et al*., 1998; *Buforn et al*., 2004; *Stich et al*., 2007] (Figure 1). Different source candidates have been proposed for the great Lisbon Earthquake [e.g., *Gutscher et al*., 2002; *Baptista et al*., 2003; *Gràcia et al*., 2003a; *Terrinha et al*., 2003; *Zitellini et al*., 2004, 2009; *Stich et al*., 2007], although none of these models satisfactorily accounts for the estimated magnitude of the earthquake and tsunami arrival times onshore.

[7] A local network of 24 broadband ocean bottom seismometers deployed in the area during a year recorded numerous small-to-moderate magnitude earthquakes ($M_L = 2.2$–4.8) that concentrate at a depth of 40–60 km, with only few events nucleating shallower than 30 km [*Geissler et al*., 2010]. Moment tensor solutions show predominantly reverse to strike-slip fault mechanisms with NW-SE oriented *P* axes [e.g., *Buforn et al*., 2004, *Stich et al*., 2005, 2007, 2010; *Geissler et al*., 2010] parallel to the maximum shortening (Sh_{MAX}) between the Eurasian and African plates (Figure 1). In this region, two main types of active faults have been recognized: (1) NE-SW trending thrusts, such as the Marquês de Pombal, São Vicente, and HFs [*Gràcia et al*., 2003a; *Terrinha et al*., 2003; *Zitellini et al*., 2004]; and (2) large WNW-ESE trending dextral strike-slip faults, such as the SFZ, which comprises a group of faults including the Lineament South (LS) [*Rosas et al*., 2009, 2012; *Terrinha et al*., 2009; *Zitellini et al*., 2009; *Bartolome et al*., 2012] (Figure 1).

3. Data and Methods

[8] This work results from the integration of acoustic and multiscale seismic data obtained in the study area and dating of scientific wells and sediment cores. Most of the data presented were acquired during the SWIM 2006 cruise, carried out onboard the Spanish RV Hesperides in the frame of the ESF EuroMargins SWIM project.

[9] Bathymetric data was obtained with a Simrad EM12S-120° multibeam system (Figure 2). Digital terrain models (50 m grid size) and slope maps were processed using the Caraibes-TD software (IFREMER, France) (Figures 2, 3a, and 3c). This dataset was merged with the EuroMargins SWIM bathymetric compilation [*Zitellini et al*., 2009] (Figure 1) and provides detailed morphostructural information. Acoustic backscatter data from the Simrad EM-120 echosounder was also acquired and processed to construct a reflectivity mosaic. In the study area, high-reflective areas (dark gray) correspond to coarse sediments (turbidites), steep slopes and/or rock outcrops whereas low-reflectivity areas (pale gray) correspond to hemipelagic sediments (Figure 3b). Furthermore, with the aid of high-resolution (1–5.5 kHz) Simrad TOPAS PS18 parametric sounder, we obtained stratigraphic and tectonic information from the uppermost tens of meters (50–80 m) below the seafloor.

[10] A grid of 11 MCS profiles (spaced ~7 nm) from the SWIM 2006 dataset (Figure 2) was used to characterize the geometry and kinematics of the newly identified structures and to constrain the timing of deformation. The SWIM 2006 MCS profiles were acquired using a 1050 c.i.-array constituted by eight airguns towed at 6 m depth and an analogical Teledyne streamer with 2.4 km of active section consisting of 96 channels (25 m separation) towed at 7 m depth. Data were recorded at a sampling rate of 2 ms and record length was 11 s two-way travel time (TWTT) with a shot interval of 37.5 m. Ten additional MCS profiles acquired during the RIFANO 1992 [*Sartori et al*., 1994] and IAM 1993 [*Tortella et al*., 1997] surveys have also been used to complete the regional tectonic interpretation (Figure 2).

[11] Lithostratigraphic information from the Deep Sea Drilling Program (DSDP) Site 135 [*Hayes et al*., 1972], located on top of the Coral Patch Ridge and drilled down to 689 mbsf (meters below the seafloor), was used to date specific seismic horizons and to assign lithologies to the seismic units identified in the MCS profiles (Figures 4 and 5). In addition, age control of key horizons in the TOPAS profiles was established on the basis of sediment cores located in the Horseshoe (MD03–2703 and MD03–2704) and Seine abyssal plains (JC27-20) (Figure 2). Sediments consisted in an alternance between hemipelagic intervals and turbidite events [e.g., *Lebreiro et al*., 1997; *Gràcia et al*., 2010]. Calibrated ^{14}C dates reveal Holocene age sediments at the seafloor of the abyssal plains, with values of 615–725 Cal yr B.P. at 50–52 cm below the seafloor in the Horseshoe Abyssal Plain and 2355–2476 Cal yr B.P. at 3–5 cm below the seafloor in the Seine Abyssal Plain. This information is not only valuable for interpretation of TOPAS profiles but also for ascertaining the age of faults that rupture up to the seafloor.

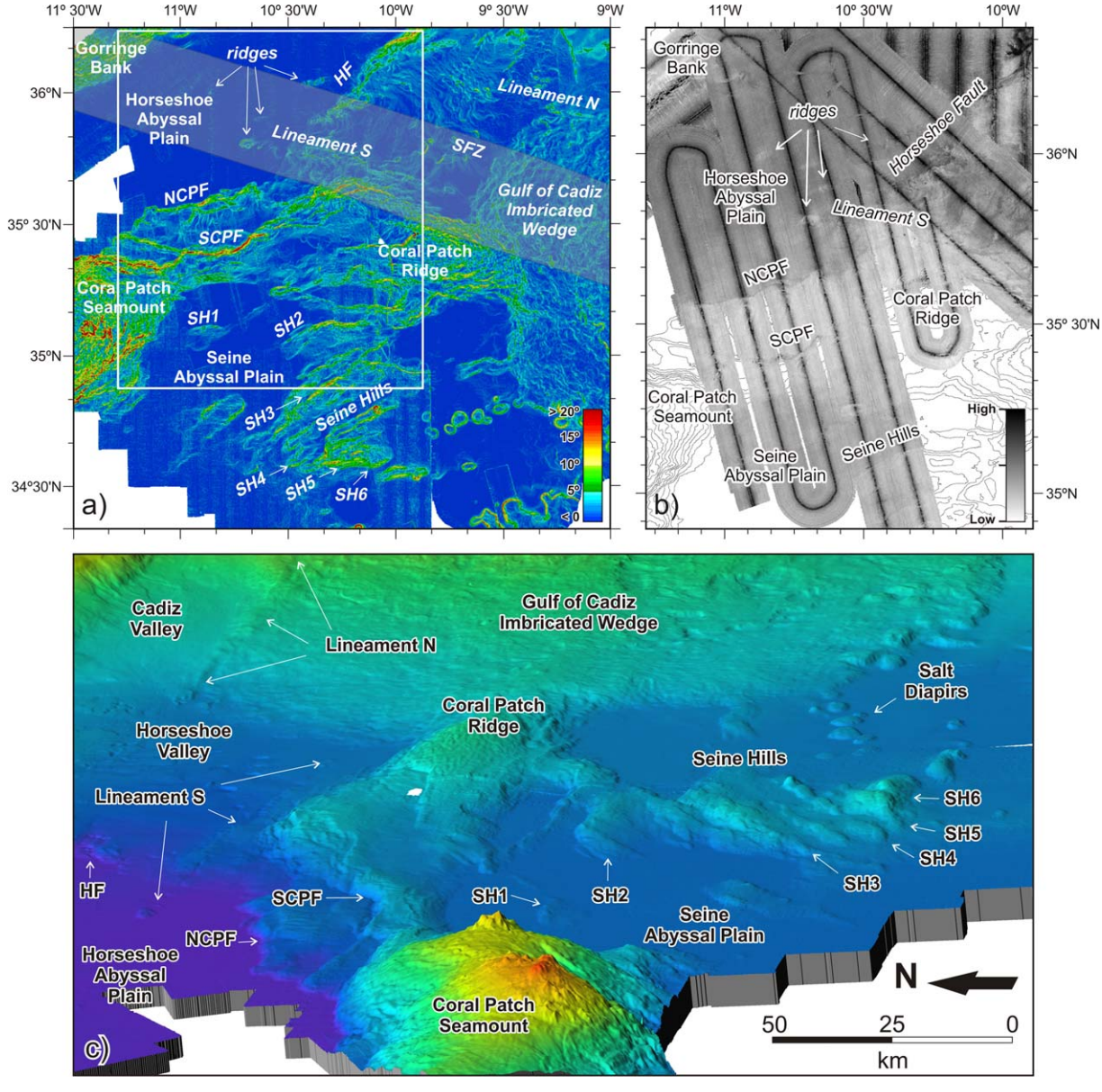

Figure 3. (a) Slope map of the external part of the Gulf of Cadiz where main features are located. The SWIM Fault Zone (SFZ) [*Zitellini et al*., 2009] is depicted as a transparent gray band. (b) Acoustic backscatter map of the Coral Patch region. High reflectivity is depicted in dark gray and low reflectivity in pale gray. White rectangle locates Figure 3b. (c) 3-D bathymetric map of the study area, view from the west. Main features are labeled. HF: Horseshoe Fault; NCP: North Coral Patch Ridge Fault; SCP: South Coral Patch Ridge Fault; SH1 to SH6: Seine Hills faults.

3.1. Seismic Processing and Interpretation

[12] Standard MCS processing was accomplished using PROMAX software, including data resampled from 2 to 4 ms, channel and shot editing, top mutes picked in the shot gather domain, true amplitude recovering, FX-decon, ensemble predictive deconvolution, and geometry common depth point reflection gather (Figure 5a). Because this work focuses on the characterization of active structures and their seismic potential, it is essential to obtain the real geometry of the structures, and this is only possible using depth-converted seismic sections. To this end, we performed a Prestack Kirchoff Depth Migration (PSDM) in four selected MCS profiles (SW03, SW07, SW13, and SW16) (Figures 2 and 5). Velocity models (Figure 5b) were constructed based on depth-focusing error analysis of the MCS data using a finite-difference ray-tracer of the SIRIUS software package (GX

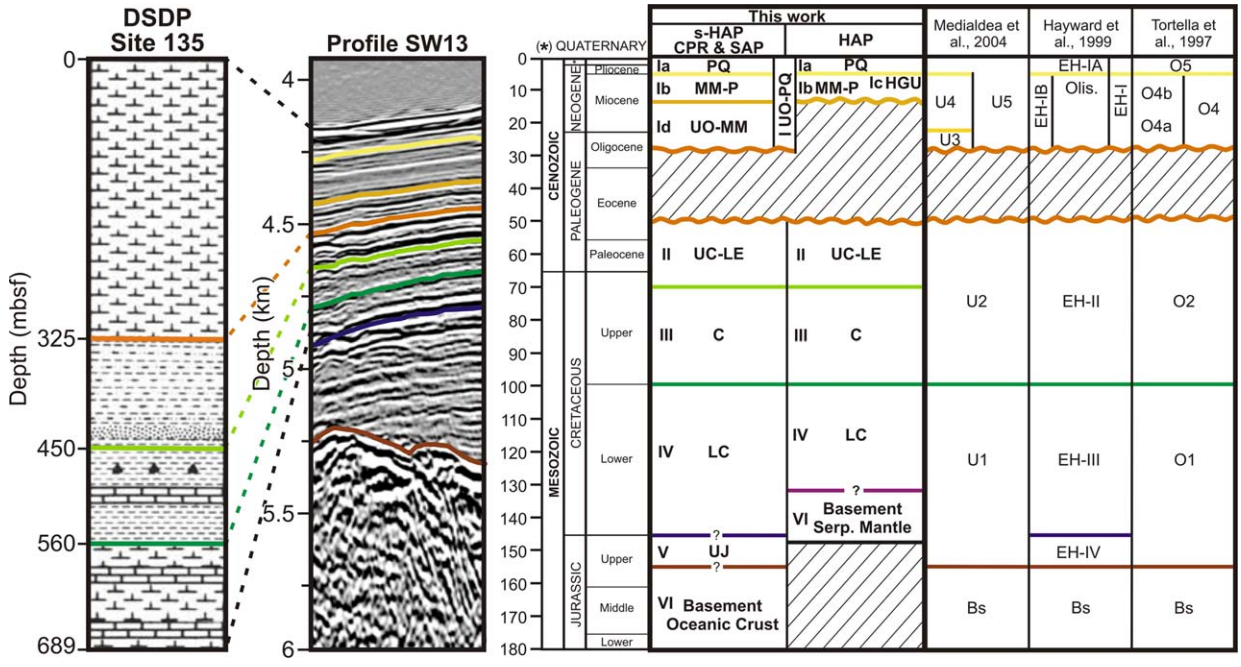

Figure 4. Seismotratigraphy based on DSDP Site 135 [*Hayes et al*., 1972] located at the intersection of pre-stack depth migrated profiles SW07 and SW13 (see Figure 2). Units previously defined by *Tortella et al*. [1997], *Hayward et al*. [1999], *Medialdea et al*. [2004] in the external part of the Gulf of Cadiz have also been included for reference. mbsf: meters below the seafloor; CPR: Coral Patch Ridge; SAP: Seine Abyssal Plain; s-HAP: southern Horseshoe Abyssal Plain. I.UO-PQ: Upper Oligocene to Quaternary; Ia.PQ: Plio-Quaternary; Ib.MM-P: Middle Miocene-Pliocene; Ic.HGU: Horseshoe Gravitational Unit, Upper Miocene; Id.UO-MM: Upper Oligocene-Middle Miocene; II.UC-LE: Upper Cretaceous-Lower Eocene; III.C: Cretaceous; IV.LC: Lower Cretaceous; V.UJ: Upper Jurassic; VI and Bs: Basement; Serp.: Serpentinized.

Technology) [*McBarnet*, 2000]. An example of the resulting PSDM profile (SW13) is shown in Figure 5c. The velocity models obtained for the profiles SW03, SW07, SW13, and SW16 were used to perform the poststack Kirchoff time migration of all the profiles. This was possible because the profiles were close to each other. Finally, we used the SMT Kingdom Suite software to represent the stratigraphic and structural interpretation for the whole MCS dataset.

[13] Seismic acquisition in areas with prominent bathymetry, like our study area, can result in poor imaging, which may be aggravated depending on the sense of data gathering (toward foreland or hinterland). Folds can be distorted or partially imaged in seismic sections and poor imaging of steeply dipping fold limbs is not uncommon (Figure 6). Faults were identified in our MCS profiles by: (1) fault cutoffs: terminations of reflections or abrupt changes in reflection attributes at fault surfaces; (2) terminations of folds limbs or kink bands; and (3) direct fault plane reflections produced by changes in velocity and density across or within fault zones. Cutoffs and fault plane reflections directly constrain fault positions [e.g., *Shaw et al*., 2005] (Figure 6). At the tip of the upper flats of some thrusts faults structural wedges were identified, which contain two connected fault segments that bound a triangular, or wedge shaped, fault block. The two fault segments merge at the tip of the wedge. Slip on both faults accommodates propagation of the wedge tip and causes folding [*Medwedeff*, 1989]. Structural wedges are characterized by: (1) presence of coeval fore and back thrusts; (2) folding localized along an active axial surface pinned to the wedge tip; and (3) folds in the footwall of the backthrust that produce structural relief [*Shaw et al*., 2005] (Figure 6).

[14] We define active structures as the ones deforming the Quaternary units. In this case, our criterion is based on (a) surface ruptures generated by dip-slip and strike-slip faults, and (b) development of young folding and growth-strata configuration generated by blind-thrust faults. The ages of growth-strata define the timing of deformation. In contractional fault-related folds, growth-strata thin

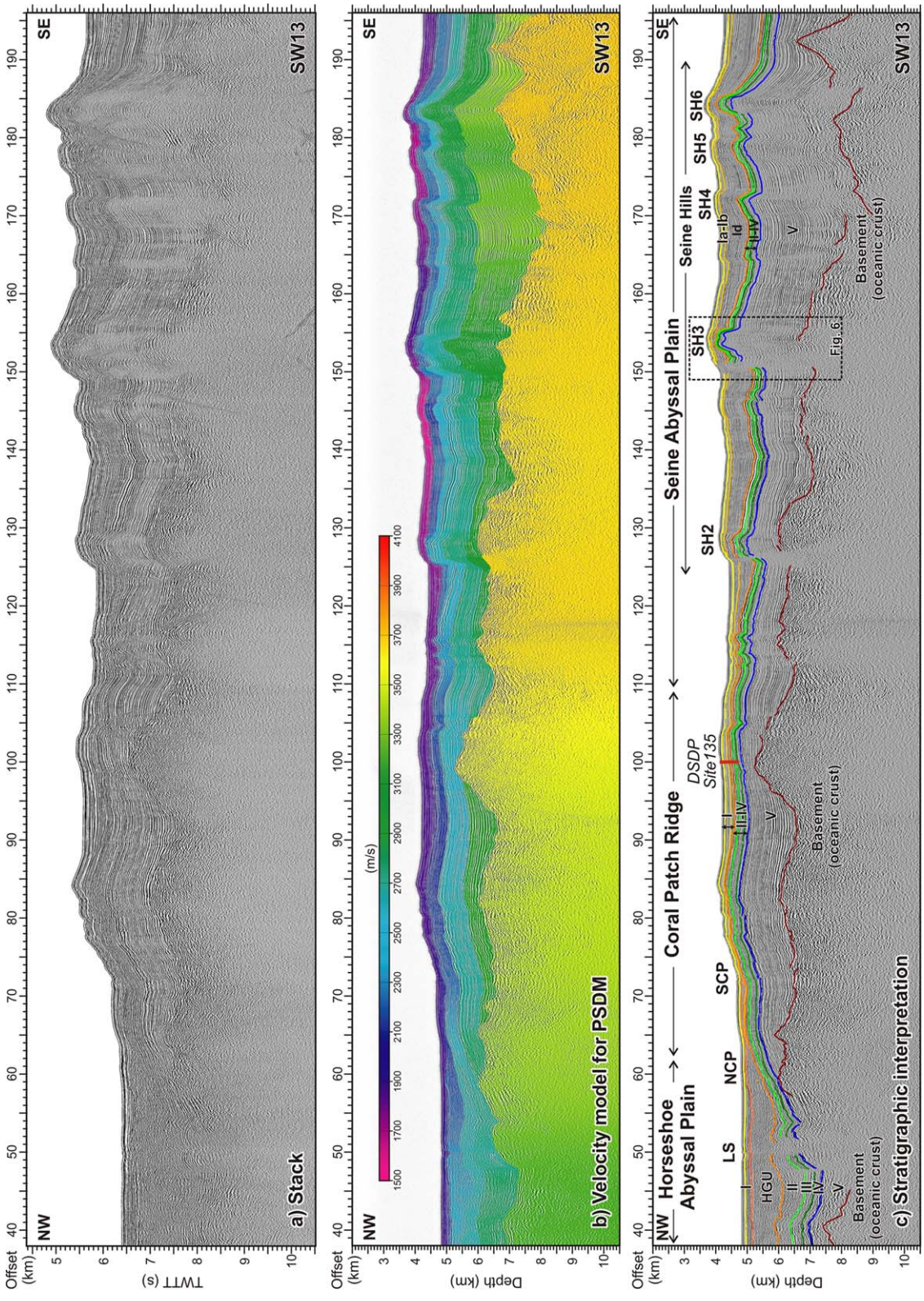

Figure 5. (a) Stack of profile SW13 based on a standard MCS processing. (b) Velocity model of the profile SW13 obtained using SIRIUS software package, which includes a depth-focusing analysis. (c) Stratigraphic interpretation of prestack depth migrated (PSDM) profile SW13. Location of seismic line in Figure 2. Black rectangle locates Figure 6. LS: Lineament South; NCP: North Coral Patch Ridge Fault; SCP: South Coral Patch Ridge Fault; SH2 to SH6: Seine Hills faults. DSDP Site 135 is located. Ages of seismostratigraphic units are in the caption of Figure 4. TWTT: Two-way travel time. Vertical exaggeration (VE) = 4.

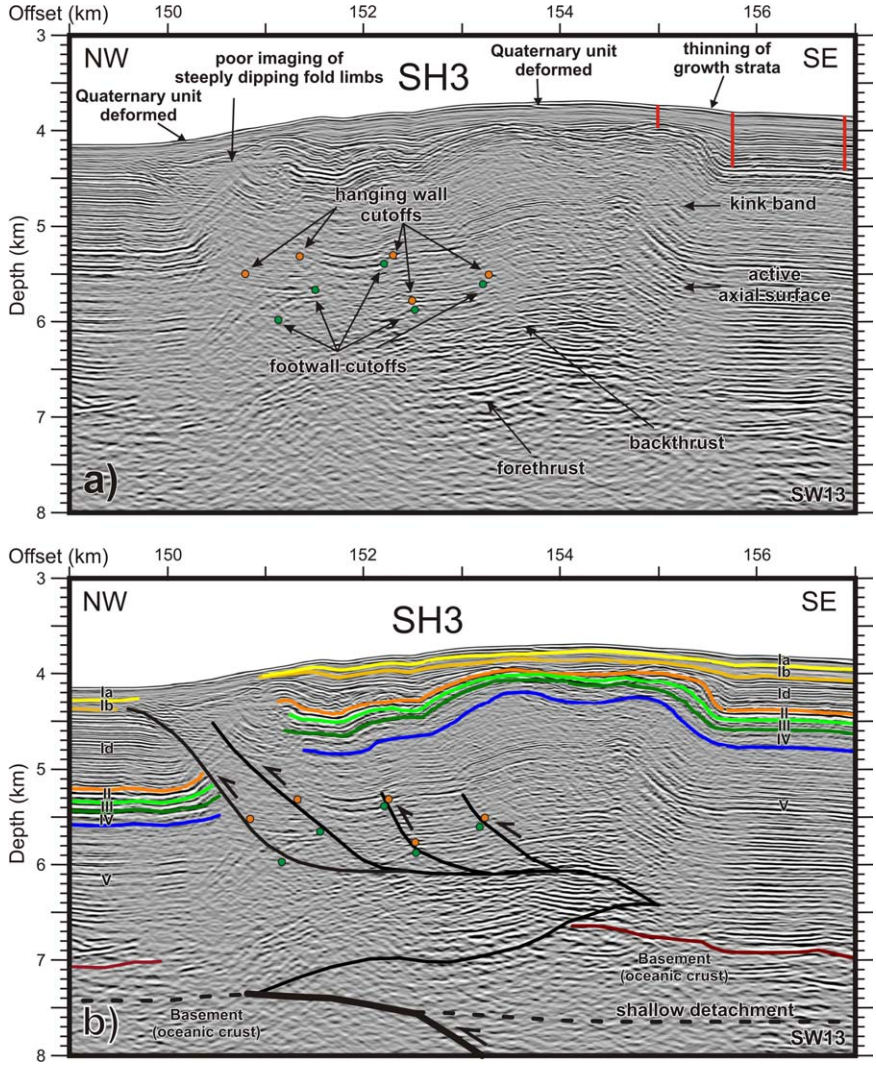

Figure 6. Prestack depth migrated (PSDM) section of MCS profile SW13 across tectonic structure SH3 (see location in Figure 5). (a) Uninterpreted section depicting the criteria followed in this study for stratigraphic and structural interpretation. Orange dots depict the hanging wall cutoffs and green dots the footwall cutoffs. Red vertical lines show the progressively thinning of the growth strata toward the structural high. (b) Tectonic and seismostratigraphic interpretation of the section. See text for details. No vertical exaggeration.

out across fold limbs and toward structural highs (Figures 5 and 6). Growth fold patterns imaged in seismic data often yield insights into the folding mechanism and sediment-to-uplift ratio positions [*Shaw et al*., 2005].

4. Morphology and Stratigraphy of the Coral Patch Ridge and Neighboring Abyssal Plains

4.1. Seafloor Morphology

[15] We characterized the three main morphostructural domains of the external part of Gulf of Cadiz (Horseshoe Abyssal Plain, Coral Patch Ridge and Seine Abyssal Plain) on the basis of high-resolution bathymetric maps (Figures 2 and 3c), slope map (Figure 3a) and backscatter data (Figure 3b). The eastern Horseshoe Abyssal Plain is a NE-SW trending 4850 m deep basin bounded to the north by the Gorringe Bank and to the south by the Horseshoe and Coral Patch Ridge faults (Figures 2 and 3c). The slope map illustrates the flat character of the Horseshoe Abyssal Plain with slopes lower than 0.1° (Figure 3a). The high/medium reflectivity in the acoustic backscatter map (Figure 3b) suggests the presence of turbidite and hemipelagic sediments in the Horseshoe Abyssal Plain, as confirmed by sediment cores

[e.g., *Lebreiro et al*., 1997; *Gràcia et al*., 2010]. In addition, groups of aligned E-W trending elongated highs, 7–16 km long, 4 km wide, and 20–165 m high are also identified (Figures 2 and 3). These ridges are visible in the slope map with gradients between 3° and 5° and can be distinguished by their lower reflectivity (Figure 3). They correspond to the westward continuation of the SWIM Faults [e.g., *Zitellini et al*., 2009; *Bartolome et al*., 2012].

[16] The Coral Patch Ridge is a rhomboidal-shaped ridge with a long E-W axis of 160 km that separates the Horseshoe Abyssal Plain from the Seine Abyssal Plain (Figures 2 and 3c). Morphologically, the Coral Patch Ridge includes two main levels: the northern and deepest (4250 m) part of the ridge, limited by the North Coral Patch Ridge (NCP) fault, and the southern and higher part (3080 m depth), bounded by the South Coral Patch Ridge (SCP) fault (Figure 3). The slope map illustrates the steep escarpments that form the ridge, with average slopes between 7° and 10° locally reaching up to 20° (Figure 3a). The top of the Coral Patch Ridge is a relatively flat area with slopes between 0.5° and 2°. In the bathymetric and slope maps we can distinguish a set of WNW-ESE linear features (50 km long, 100 m high) across the Coral Patch Ridge that are parallel to the SFZ (Figures 2, 3a, and 3c). The acoustic backscatter map reveals low reflectivity in the area, as expected for a homogeneous sedimentary cover, and higher in the steep fault scarps and rocky outcrops (Figure 3b).

[17] The northeastern part of the Seine Abyssal Plain is shallower than the Horseshoe Abyssal Plain (4450 m depth) and is limited to the north by the Coral Patch Seamount and Coral Patch Ridge and to the east by the Gulf of Cadiz Imbricated Wedge (GCIW) (Figures 1, 2, and 3c). The Seine Abyssal Plain is a flat basin with slopes close to 0° (Figure 3c) and contains several NE-SW trending elongated ridges, hereafter referred to as the Seine Hills (SH1 to SH6). The largest hill is 55 km long and the highest rises 740 m above the surrounding seafloor (Figures 2, 3a, and 3c). The Seine Hills have slopes between 4° and 20° and moderate reflectivity (Figure 3a and 3b). Other features include some WNW-ESE trending lineaments (55 km long, 5 km wide) that are subparallel to the SFZ, although fewer than in the Coral Patch Ridge area (Figures 2 and 3). In the eastern part of the Seine Abyssal Plain, circular salt diapirs (4–8 km diameter) are also observed, rising between 100 and 200 m above the seafloor (Figures 2 and 3).

4.2. Seismostratigraphy

[18] Seismostratigraphic units have been correlated with units that were previously defined in the area [*Tortella et al*., 1997; *Hayward et al*., 1999; *Medialdea et al*., 2004] as well as with the DSDP Site 135 [*Hayes et al*., 1972] (Figure 4), which is crossed by two of the PSDM seismic profiles (SW07 and SW13) (Figures 2 and 5). The unprecedented higher resolution of the SWIM 2006 MCS dataset enabled us to revise the existing units and to define new subunits and seismic horizons in the first km below the seafloor (Figures 4 and 5). From top to bottom, the following six seismostratigraphic units (I–VI) were defined.

4.2.1. Unit I: Upper Oligocene to Quaternary

[19] This unit (0–325 m below the seafloor) is composed of light gray nannoplankton chalk ooze and pelagic carbonates interbedded with sandy layers [*Hayes et al*., 1972]. Within this unit, we identified three major discontinuities separating four subunits (Ia, Ib, Ic, and Id) with a distinctive seismic character: Ia—PlioQuaternary. This is characterized by parallel reflectors of low-medium amplitude and discontinuous reflectors toward its base; Ib—Middle Miocene-Pliocene. The seismic facies of this subunit is variable, from low-amplitude and semicontinuous reflectors in the Coral Patch Ridge and Seine Abyssal Plain to higher amplitude and continuous reflectors in the Horseshoe Abyssal Plain; Ic—Horseshoe Gravitational Unit (HGU). This subunit corresponds to a large allochthonous body emplaced during the Upper Miocene (Tortonian), tapering out the underlying subunit [e.g., *Torelli et al*., 1997; *Tortella et al*., 1997; *Hayward et al*., 1999; *Medialdea et al*., 2004; *Zitellini et al*., 2004; *Iribarren et al*., 2007]. The HGU is a regional marker observed throughout the Horseshoe Abyssal Plain and is characterized by high-amplitude chaotic facies with numerous diffractions and hyperbolic reflections. Few internal reflectors can be identified; Id—Upper Oligocene—Middle Miocene. This subunit is observed in the Coral Patch Ridge and Seine Abyssal Plain, but rarely in the Horseshoe Abyssal Plain. It shows parallel, continuous well-stratified, high-amplitude reflectors and onlaps the underlying unit. The top and bottom are high-amplitude horizons corresponding to regional unconformities (Figures 4 and 5).

4.2.2. Unit II: Upper Cretaceous (Maastrichtian) to Lower Eocene

[20] This unit (325–450 m below the seafloor) is composed of terrigenous sediments and limestones at its base [*Hayes et al*., 1972]. It presents continuous and high-amplitude reflectors that change to discontinuous and lower amplitude ones toward its base. The top is constituted by a prominent unconformity marked by a continuous high-amplitude reflector that corresponds to a sedimentary hiatus from the Lower Eocene to Upper Oligocene (Figures 4 and 5).

4.2.3. Unit III: Cretaceous

[21] This unit (450–650 m below the seafloor) is composed of green and black shales interbedded with limestone, silt and chert layers [*Hayes et al*., 1972]. It is characterized by parallel, semicontinuous, low-amplitude to transparent reflectors. A high-amplitude horizon at the base of the unit represents a major unconformity of Aptian age (Figures 4 and 5).

4.2.4. Units IV and V: Lower Cretaceous–Upper Jurassic

[22] The oldest unit drilled at the DSDP Site 135 was Unit IV (Lower Aptian, 650–689 m below the seafloor), which is composed of olive gray and black marls and limestones [*Hayes et al*., 1972]. Unit V has been assigned an age of 155–180 million years (Upper Jurassic) [*Hayes et al*., 1972]. In the Coral Patch Ridge and Seine Abyssal Plain both units are restricted to V-shaped basins and their seismic character is very variable, showing parallel reflectors onlapping the top of basement ridges. In the Horseshoe Abyssal Plain, Unit IV overlies the basement (Figures 4 and 5).

4.2.5. Unit VI: Basement

[23] This unit can be divided into two types according to their origin and present-day structural pattern. In the southernmost part of the Horseshoe Abyssal Plain, the Coral Patch Ridge and the Seine Abyssal Plain, the basement is interpreted to be made of Jurassic-age oceanic crust based on WAS, MCS, and magnetic data [*Contrucci et al*., 2004; *Rovere et al*., 2004; *Martínez-Loriente et al*., 2011]. In these areas, the basement is structured in half-grabens and is characterized by high-amplitude reflectors with poor lateral continuity that become weaker, chaotic and more diffracted with depth. In contrast, recent WAS data modeling suggests that the basement of the northern part of the Horseshoe Abyssal Plain is made of partially serpentinized peridotite that was exhumed by passive mantle denudation in the Lower Cretaceous [*Sallarès et al*., 2013].

5. Tectonic Structure of the Coral Patch Ridge and Neighboring Abyssal Plains

5.1. Eastern Horseshoe Abyssal Plain

[24] Several MCS profiles show the sedimentary infill of the eastern part of the Horseshoe Abyssal Plain (Figures 2, 5, and 7). Maximum thickness of the units is attained in the centre of the plain, decreasing toward the edges of the basin. Most of the acoustic basement (Unit VI) of the Horseshoe Abyssal Plain has been interpreted to be made of serpentinized mantle [e.g., *Sallarès et al*., 2013], and displays a very irregular upper surface at a depth between 2 and 5.5 km below the seafloor in profile SW13. However, preliminary modeling of WAS data suggests that the basement at the southernmost part of the Horseshoe Abyssal Plain and at the footwalls of the HF and Coral Patch Ridge, might correspond to oceanic crust [*Martínez-Loriente et al*., 2011]. Overlying, a well-developed Unit V (~1 km thick) is present (Figures 5, 7a, 8a, and 8b). Unit IV has a variable thickness, with a maximum of ~1.7 km in profile SW03. Mimicking the top surface of Units IV, III, and II deepen toward the centre of the basin and have more constant thicknesses of ~400 m. The upper boundary of Unit II corresponds to an erosive surface generated by excavation and erosion during the emplacement of subunit Ic (HGU), which fills the basin (maximum thickness of 1.7 km in SW13) and pinches out toward the edges of the Horseshoe Abyssal Plain (Figures 5, 7, and 8). Profile SW03 shows how the reverse HF and related splay faults uplift the entire sedimentary sequence (i.e., about 800 m of vertical offset in Unit IV), indicating major basement involvement in the structure (Figure 7a).

[25] On the basis of their activity, two main families of subvertical faults are observed in the Horseshoe Abyssal Plain: (a) those affecting the Mesozoic up to Lower Eocene sediments; and (b) those that deform all the sedimentary sequence from the basement to the seafloor (Figure 7). In the former case, we refer to tectonic structures of little entity that generate folds, discontinuities and small vertical displacements within the Mesozoic Units, although few of the structures deform the sediments up to the top of Unit II (Figure 7). The later family is characterized by subvertical faults that cut, fold and displace the whole sedimentary sequence up to the seafloor, generating small (<16 km long, <160 m high), elongated hills observed in the Horseshoe Abyssal Plain (Figure 3). Most of

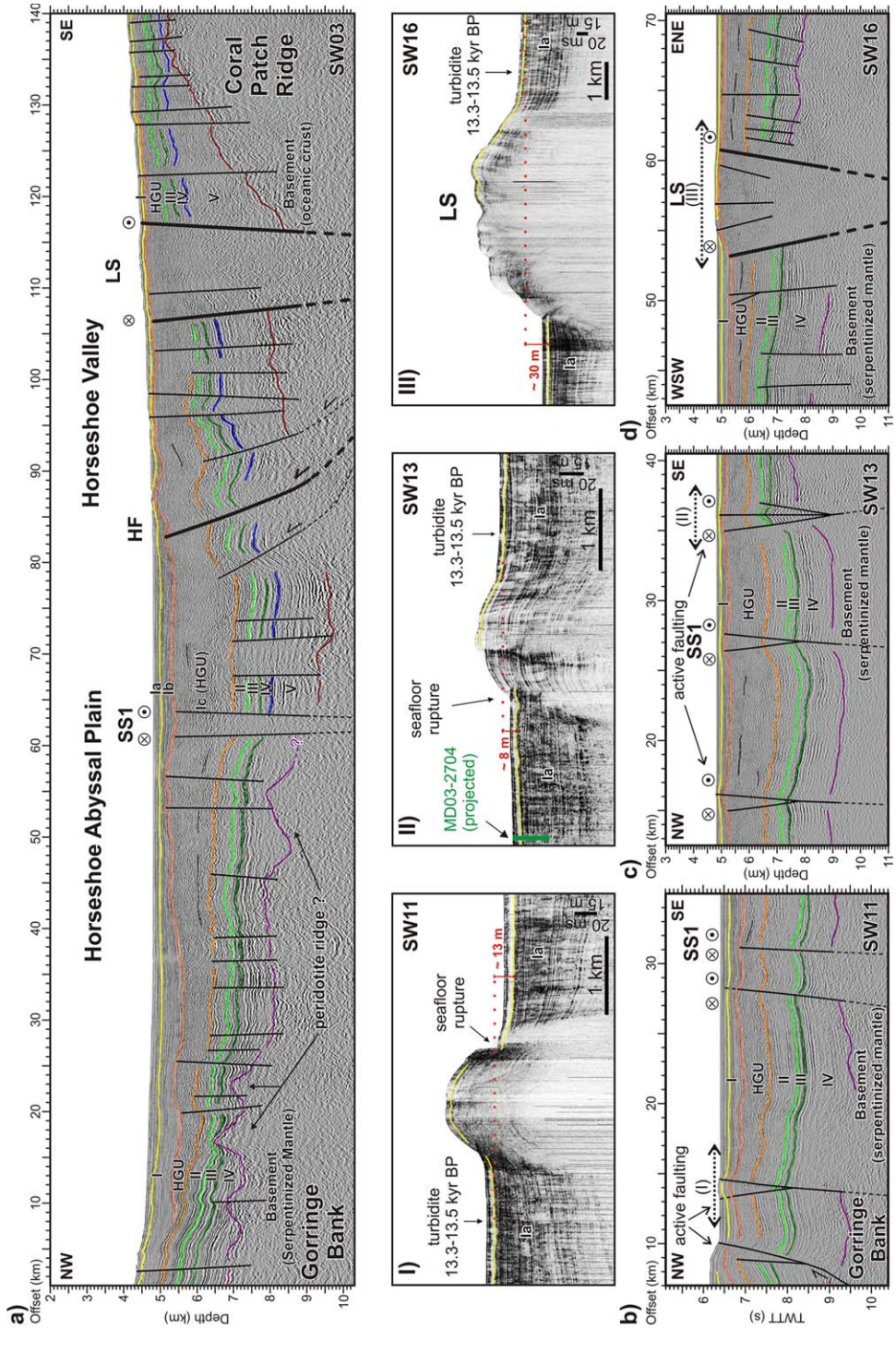

Figure 7. (a) Interpreted prestack depth migrated (PSDM) profile SW03 across the Horseshoe Abyssal Plain (HAP) from the Gorringe Bank to the Coral Patch Ridge (CPR), which intersects the Horseshoe Fault (HF), the Lineament South (LS), and the Strike-slip Fault 1 (SS1). VE = 4. (b) Interpreted section of the time-migrated profile SW11 in the northern sector of the HAP showing active strike-slip faulting (among them, SS1). The dashed arrow marks the location of Section I: TOPAS profile showing the surface expression of a positive flower structure. The yellow horizon underlines the base of a thick transparent unit, corresponding to a regional, <5 m thick turbidite event of Late Pleistocene age (13.3–13.5 Cal kyr BP) on the basis of radiocarbon dating of core MD03–2704 [*Gràcia et al.*, 2010]. The maximum vertical offset (13 m) of the turbidite layer across the fault is depicted. (c) Interpreted section of the PSDM profile SW13 across the central part of the HAP showing three active strike-slip faults (among them, SS1). The dashed arrow marks the location of Section II: TOPAS profile across a positive flower structure showing surface rupture. The maximum vertical offset (~8 m) of the turbidite is depicted. (d) Interpreted section of the PSDM profile SW16 across the LS in the eastern part of the HAP. The dashed arrow marks the location of Section III: TOPAS profile across LS showing a maximum vertical offset (30 m) of the turbidite layer. Location of MCS and TOPAS profiles in Figure 2. Ages of seismostratigraphic units are in the caption of Figure 4. Nature of the basement is inferred from *Sallarès et al.* [2013]. TWTT: Two-way travel time. MCS profiles (Figure 7b–7d) VE = 2; TOPAS profiles (Sections I–III) VE = 20.

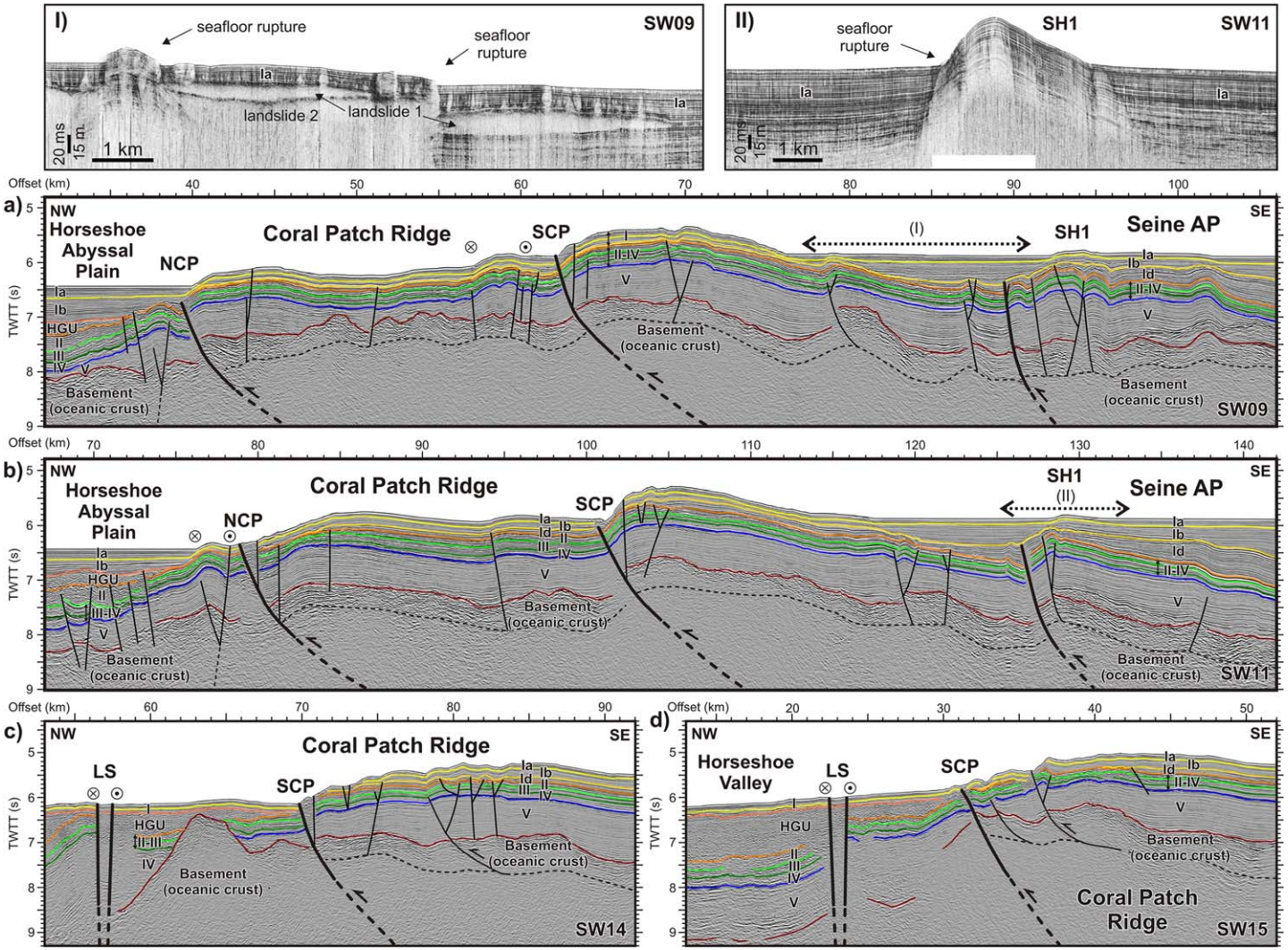

Figure 8. (a) Interpreted section of the time migrated profile SW09 across the western part of the Coral Patch Ridge (CPR), from the Horseshoe Abyssal Plain (HAP) to the Seine Abyssal Plain (SAP). The North Coral Patch Ridge (NCP) and South Coral Patch Ridge (SCP) thrusts faults and the Seine Hill 1 (SH1) transpressive structure are imaged. The dashed arrow marks the location of Section I: TOPAS profile showing a landslide succession laterally offset by a vertical fault with surface expression. (b) Interpreted section of the time migrated profile SW11 crossing the central part of the Coral Patch Ridge, from the Horseshoe to the Seine abyssal plains. The NCP, SCP and SH1 thrusts are imaged. The dashed arrow marks the location of Section II: TOPAS profile across SH1 showing a seafloor rupture. (c) Interpreted section of the time migrated profile SW14 at the eastern part of the Coral Patch Ridge crossing Lineament South (LS) and SCP. (d) Interpreted section of the time migrated profile SW15 at the eastern end of the Coral Patch Ridge across LS and SCP faults. See text for details. Location of MCS and TOPAS profiles in Figure 2. Ages of seismostratigraphic units are in the caption of Figure 4. TWTT: Two-way travel time. MCS profiles (Figure 8a–8d) VE = 2; TOPAS profiles (Sections I and II) VE = 20.

these structures show flower-like geometries characteristic of strike-slip faults. However, as some of them show a dip-slip component, transpressive behavior can also be proposed (Figure 7). Profile SW13 shows how some of these faults produce a significant vertical displacement (i.e., 600 m at the top of Unit IV), progressively decreasing its offset from the top of the basement to Unit I (e.g., SS1 in Figure 7c). The most prominent of these active faults corresponds to the LS, a WNW-ENE trending dextral strike-slip fault that extends for 180 km across the Horseshoe Abyssal Plain and part of the GCIW (Figures 1–3) [e.g., *Zitellini et al*., 2009; *Bartolome et al*., 2012]. The LS corresponds to a 2–4 km wide fault zone with transparent seismic facies that is bounded by subvertical faults that cut across the entire sedimentary sequence from at least 11 km deep up to the seafloor. The LS produces approximately 500 m of vertical displacement of the top of Unit IV and 200 m of the top of Unit II (Figure 7d).

[26] TOPAS profiles provide evidence of the surface expression of the subvertical faults and the LS across the Horseshoe Abyssal Plain, showing 2–4 km wide anticlines bounded by fault surface ruptures (Figure 7, Sections I–III). These active strike-slip faults vertically displace a widespread, 3–5 m thick horizon of transparent facies corresponding to the turbidite event E13 (Figure 7, Sections I–III), whose age is 13,350–13,505 Cal yr B.P. based on ^{14}C dating of cores MD03–2703 and MD03–2704 [*Gràcia et al*., 2010]. This allows us to calculate a maximum cumulative vertical slip-rate of these subvertical faults since the late Pleistocene, which is 0.6–0.9 mm/yr for the first two and about 2.2 mm/yr for the LS (Figure 7, Sections I–III).

5.2. Coral Patch Ridge

[27] The acoustic basement of the Coral Patch Ridge is characterized by tilted blocks of oceanic crust originally structured in half-grabens and generating an irregular topography [*Martínez-Loriente et al*., 2011]. The top of the basement is located between 1.2 km and 2.4 km depth below the seafloor (Figure 5). Unit V sediments infill the wedge-like depocenters generated during the rotation of the half-grabens, and develop progradational configurations on the hanging walls and aggradational packages at the top of footwalls (Figures 5 and 8). This gives rise to large variations in thickness, from 1500 m at the half-grabens to 400 m at the top of the footwalls. The overlying Units IV to II are characterized by a relatively constant thickness (100–240 m thick) throughout the area, although they are thinner when compared to the same units in the Horseshoe Abyssal Plain (Figures 5 and 8).

[28] The Coral Patch Ridge is formed by two main NW-verging anticline thrust faults: the 65 km long NCP fault and the 83 km long SCP fault (Figures 3 and 8). These thrusts are characterized by backlimbs that dip less than the fault-ramp and forelimbs that are quite narrow in relation to their long backlimbs, suggesting that they were generated by shear fault-bend folding [*Suppe et al*., 2004]. The seismic images show the ramps of the fault-bend folding thrusts, whereas the lower flats are probably located below the window of acquisition. The grid of MCS profiles across Coral Patch Ridge allowed us to characterize the lateral variation of these two sets of thrusts that uplifted the ridge. The westernmost profiles (e.g., SW09) show the NW-verging NCP fault as a blind thrust, displacing and folding the whole stratigraphic sequence up to the Plio-Quaternary subunit Ia (Figures 2 and 8a). The profiles across the central part of the Coral Patch Ridge (e.g., SW11) show how the NCP fault reaches up to the seafloor (Figure 8b) and the easternmost profile (SW13) depicts the fault termination to the east. The vertical displacement generated by the NCP fault displays maximum offset values in the central part, 500 ms (TWTT) for the top of Unit V and 420 ms (TWTT) for the top of Unit II (Figure 8b). The SCP thrust fault has a NW-ward sense of displacement, folding and uplifting the southeastern hanging-wall fault block, and cutting through the whole stratigraphic sequence up to the seafloor (Figure 8). The vertical slip of the SCP fault is relatively constant with an average value of 540 ms (TWTT) for different horizons, such as the top of Units V, II, and I. Both thrusts (NCP and SCP faults) show higher fault dips within the first km below the seafloor (average 40°), decreasing within the basement (average 25°) (Figure 8).

[29] Minor subvertical to normal faults locally affects the top of the anticlines. A secondary active thrust south of the SCP fault is observed in profiles SW14 and SW15 (Figures 8c and 8d) with little vertical displacement. This thrust would propagate from a shallow depth detachment layer located at the uppermost part of the oceanic crust. Finally, the Coral Patch Ridge region is also affected by active positive strike-slip flower structures (Figure 8a) and transpressive subvertical faults that affect the sedimentary sequence from the basement to subunit Id (Mid-Miocene),

generating folds and small vertical displacements. Most of these structures would also be rooted in the shallow detachment layer mentioned above. Buckle folds have been identified at the front of NCP and SCP thrusts (Figure 8).

5.3. Northern Seine Abyssal Plain

[30] In this part of the Seine Abyssal Plain, the acoustic basement is also structured in half-grabens as imaged in the MCS profiles (Figures 8a, 8b, and 9). The top of the basement deepens toward the SE, at about 5 km depth below the seafloor in the southern Seine Hills area (Figure 9). Unit V infilled the original grabens and show large thickness variations, with a maximum of ~4 km thick in the basin located between SH4 and SH5 (Figure 9). Units IV to II are concordant with the underlying Unit V and are thin, with a fairly constant thickness (~400 m) in the whole Seine Abyssal Plain area. In contrast, the onlapping subunit Id, which is exceptionally thick, shows a maximum thickness south of SH6 (1 km thick) that progressively thins out toward the NE (150 m thick). Subunits Ia and Ib are parallel and are of relatively constant thickness in the Seine Hills area, although the thickness of subunit Ib locally increases (~750 m) north of SH2 and south of SH6 (Figure 9).

[31] The northeastern Seine Abyssal Plain region is also characterized by two types of faults: (1) NE-SW trending reverse faults; and (2) WNW-ESE trending strike-slip faults. The former faults are referred to as the Seine Hills, which is a succession of ridges (SH2 to SH6) that correspond to NE-SW trending thrust-folds with NW and SE vergences (Figure 9). These thrusts may have developed by fault-bend folding (e.g., SH2 and SH3) [*Suppe*, 1983] or by fault-propagate folding (e.g., SH5) [e.g., *Allmendinger*, 1998]. At the tip of the upper flats of these thrusts, structural wedges (or triangle zones) [*Medwedeff*, 1989] were developed, having generated associated back-thrusts and kink folds that accommodate the shallow deformation near the seafloor (Figures 6 and 9). In the case of the fault-propagation folds (e.g., SH5), the MCS images show asymmetric folding with narrow and steep forelimbs in contrast to their corresponding backlimbs. The SH4 and SH5 are structured as a "classic" trishear fault-propagation fold formed by distributed shear within a triangular zone that expands outward from a fault tip [*Erslev*, 1991]. In the case of the SH6, a trishear fault-propagation-fold developed at its tip on the NW side, and shows a wedge structure at depth. Furthermore, the SH6 may involve a basement normal fault (i.e., oceanic crust) reactivated as reverse (Figure 9). In general, the Seine Hills faults deform all the units from the oceanic crust to the uppermost Quaternary sediments by faulting, blind faulting or folding, and originate >450 m high, ~50 km long reliefs as observed on the bathymetric maps (Figures 2 and 3). The Seine Hills faults (SH2 to SH6) show a higher dip (average 45°) decreasing from the subsurface to the basement (Figure 9), where the fault ramps tend to flatten (20–30°), probably toward the base of the crust (Figure 10). Unfortunately, the lower flats of the thrusts could not be imaged by our MCS acquisition system. On the basis of the PSDM profile SW13, which runs across the central part of the Seine Hills, we calculated the vertical displacement generated by these faults. The vertical offset is constant for the top of the Units V to II, and corresponds to 650 m for SH2, 1350 m for SH3, 400 m for SH4, and 250 m for SH5 (Figure 9). Although the Seine Hills are mainly blind thrusts, the growth-strata configuration of the youngest sediments confirms the present-day activity of these faults (Figure 6).

[32] Between the major Seine Hills thrusts, secondary blind thrusts showing kink-folds and asymmetric folds are also imaged and likely root in a common shallow detachment level that continues toward the Coral Patch Ridge area (Figures 8 and 9). The SH1 is a 38 km long isolated hill located west of the SH2-SH6 succession (Figure 3). According to its morphological expression and internal geometry, we distinguish two main segments corresponding, from west to east, to an 18 km long, W-E trending transpressive fault (profile SW09, Figure 8a), and a 20 km long, NE-SW trending reverse fault (profile SW11, Figure 8b). The strike-slip segment is characterized by subvertical faults defining a positive flower structure, whereas the thrust segment shows a fault with lower dip (45°), which flattens (20°) at the basement (Figure 8). Both SH1 segments fault and fold the sedimentary sequence from the basement up to the seafloor (Figures 8a and 8b). TOPAS data across the eastern segment of the SH1 show a surface rupture and anticline generated by the thrust fault (Figure 8, Section II).

[33] The strike-slip faults are mainly located north of the Seine Hills. In the MCS profiles, they are imaged as subvertical faults developing positive flower-like structures and showing seafloor ruptures in the TOPAS profiles (Figure 8a, Section I

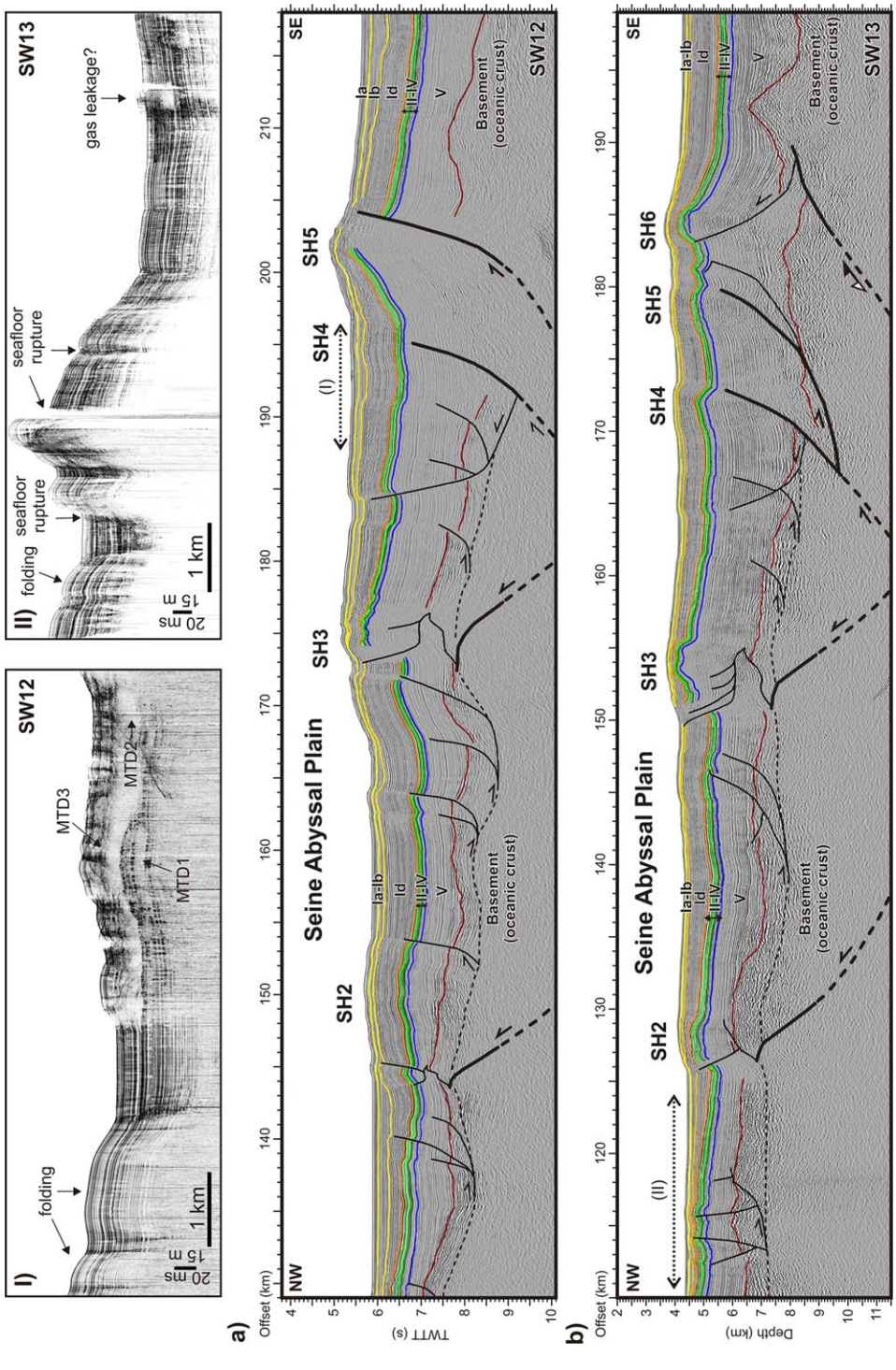

Figure 9. (a) Interpreted section of the time migrated profile SW12 across the tectonic structures of the Seine Hills (SH2 to SH6). The dashed arrow marks the location of Section I: TOPAS profile across the basin located between SH3 and SH4, where a succession of mass transport deposits (MTD) is located at the foot of SH4. (b) Interpreted section of the PSDM profile SW13 across a set of strike-slip faults in the northern part of the section and across the Seine Hill faults (SH2 to SH6). The dashed arrow marks the location of Section II: TOPAS profile across a set of narrowly spaced subvertical strike-slip faults showing seafloor ruptures. Location of MCS and TOPAS profiles in Figure 2. Ages of seismostratigraphic units are given in the caption of Figure 4. TWTT: Two-way travel time. MCS profiles (Figures 9a and 9b) VE = 2; TOPAS profiles (Sections I and II) VE = 20.

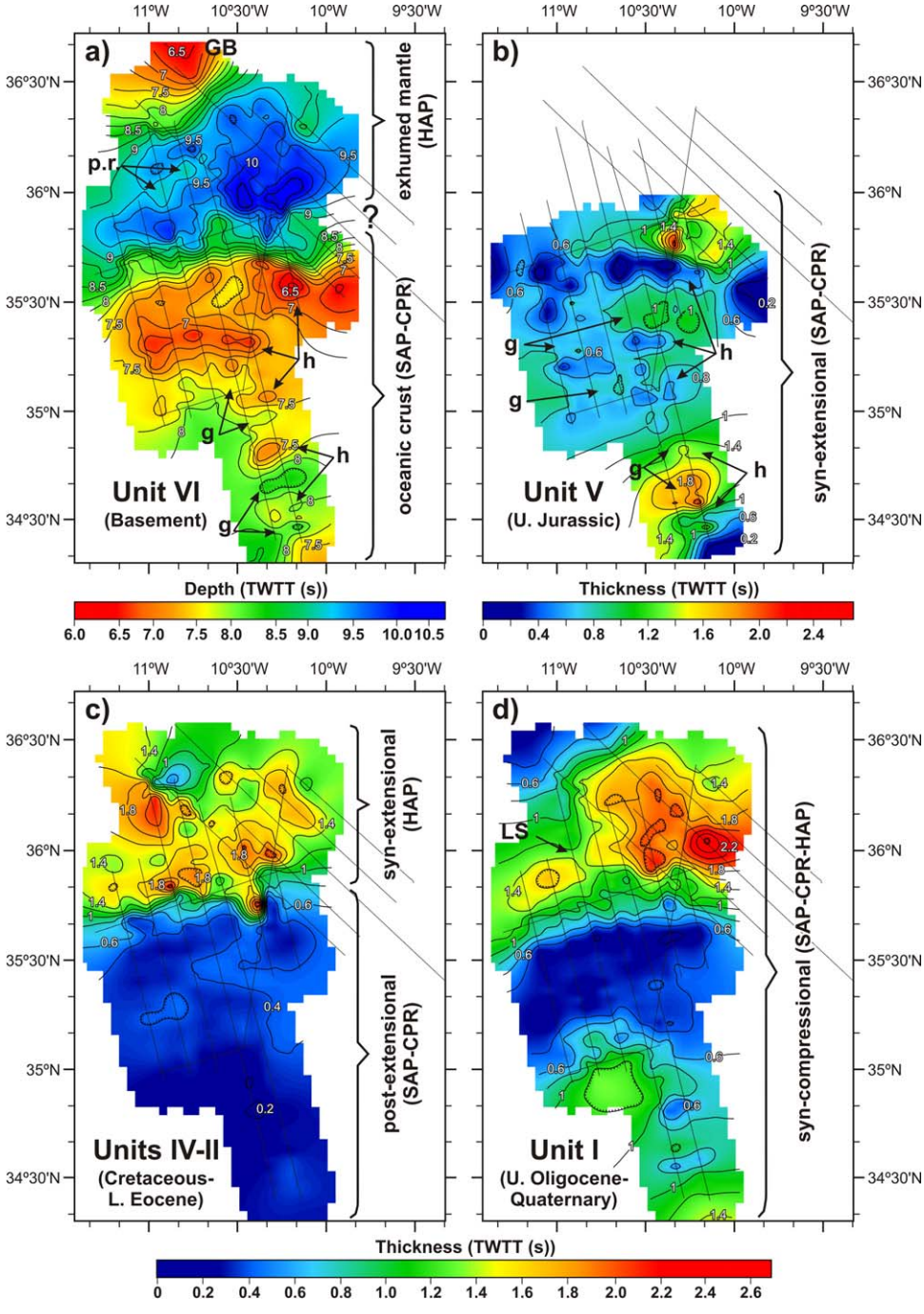

Figure 10. (a) Map of the topography of Unit VI (basement) in seconds (TWTT). (b–d) Isochore maps in seconds (TWTT) of Unit V (Upper Jurassic), Units IV-II (Cretaceous to Lower Eocene), and Unit I (Upper Oligocene to Quaternary), respectively. The Horseshoe Abyssal Plain (HAP), the Coral Patch Ridge (CPR), and the Seine Abyssal Plain (SAP) domains are identified. The SWIM 2006 profiles are depicted as thin black lines. GB: Gorringe Bank; g: graben; h: horst; LS: Lineament South; p.r.: peridotite ridge.

and Figure 9a, Section II). In addition, slope failures probably related to the activity of the neighboring faults are also identified. They show characteristic transparent seismic facies in the TOPAS profiles, such as the mass transport deposits located near SH1 and SH5. For instance, in the small basin located between the SCP and SH1 faults, a large mass transport deposit (7 km wide and up to 15 m thick) is offset by a vertical fault reaching up to the seafloor (Figure 8, Section I).

Further evidence of mass wasting is located in the basin north of SH5, where a succession of three mass transport deposits has also been identified (Figure 9, Section I).

6. Discussion

6.1. Geodynamic Evolution of the Coral Patch Ridge Region

[34] The Gulf of Cadiz has undergone successive deformation phases corresponding to the evolution of the African, Iberian, and Eurasian Plate boundaries since the initial rifting of the Central and North Atlantic [e.g., *Schettino and Turco*, 2009]. We relate our results to the main kinematic phases and propose a geodynamic evolution of the Coral Patch Ridge region. To illustrate the tectonosedimentary evolution of the area, we produced a basement and isochore (i.e., equal vertical thickness) time maps (in seconds TWTT) of the seismostratigraphic units associated with the three main deformation phases (Figure 10). In addition, we present a regional cross section from the Horseshoe to the Seine abyssal plains synthesizing the relationship between the seismostatigraphic units and main tectonic structures (Figure 11).

[35] According to regional geodynamic reconstructions [*Schettino and Turco*, 2009], the oceanic crust conforming the basement of the Coral Patch Ridge and the Seine Abyssal Plain areas was probably generated during the early stages of seafloor spreading of the northeastern segment of the Central Atlantic (i.e., Jurassic), [e.g., *Contrucci et al*., 2004; *Rovere et al*., 2004; *Martínez-Loriente et al*., 2011]. The rifting process resulted in tilted, extensional blocks following a horst and graben architecture, as observed in the MCS profiles (Figures 8, 9, and 11). On the basement map of this area, we identify a topographically elevated area in the Coral Patch Ridge and a succession of ~E-W-aligned elongated highs and lows, likely related to the original host-and-graben structure (Figure 10a). The exhumed mantle rocks, inferred to underlie the sedimentary pile of most of the Horseshoe Abyssal Plain, appear to have been exhumed in the early opening of the North Atlantic during the Lower Cretaceous [*Schettino and Turco*, 2009; *Sallarès et al*., 2013] (Figures 7 and 11). The basement map of the Horseshoe Abyssal Plain domain reflects a very irregular surface, with a large topographic low and locally elongated highs interpreted as

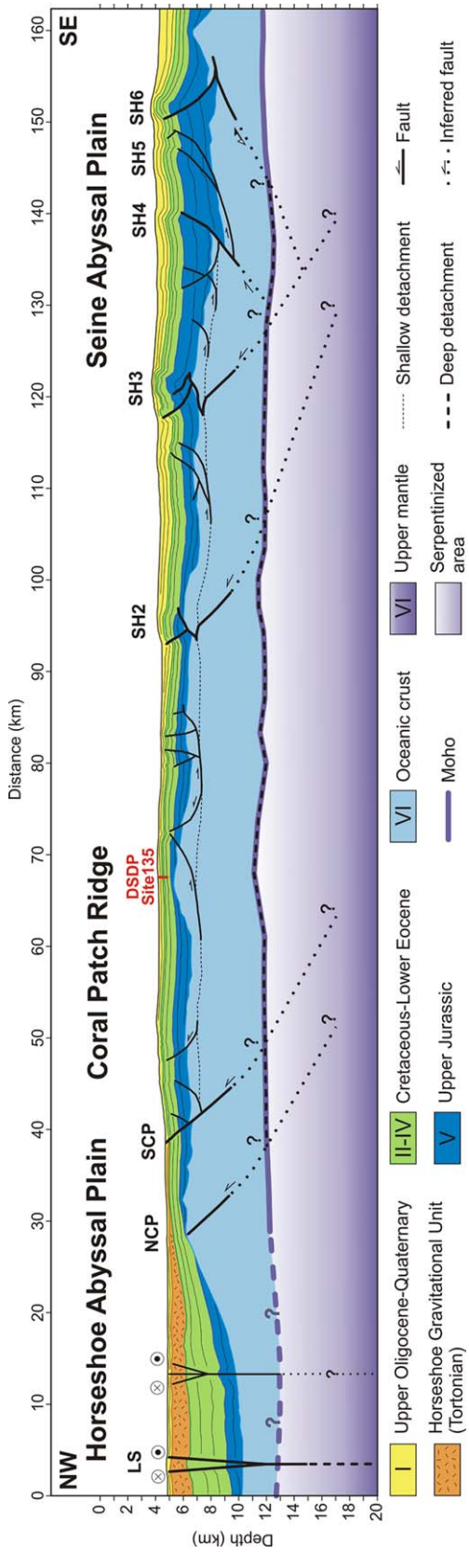

Figure 11. Regional tectonic and stratigraphic synthetic cross-section through the study region extending from the eastern Horseshoe Abyssal Plain to the northern Seine Abyssal Plain. The main sedimentary sequences and tectonic structures, such as the strike slip (LS) and thrust faults (NCP, SCP, SH2 to SH6) are imaged. LS: Lineament South, NCP: North Coral Patch Ridge Fault; SCP: South Coral Patch Ridge Fault; SH: Seine Hills faults. VE = 1.5.

peridotite ridges. Toward the NW, a high bounded by steep slope corresponds to the base of the Gorringe Bank (Figures 7a and 10a).

[36] Units V to II were deposited as the Atlantic rift-drift transition continued during the Upper Jurassic to the Lower Eocene [*Schettino and Turco*, 2009]. Their terrigenous composition suggests deposition in an abyssal plain environment [*Hayes et al*., 1972]. Unit V, present at the Coral Patch Ridge, Seine Abyssal Plain, and locally at the southernmost Horseshoe Abyssal Plain, infills depressions between tilted basement blocks with growth-strata configuration, suggesting that sedimentation took place synchronously with the extension of the NE segment of the Central Atlantic (Figures 8, 9, and 11). In the isochore map of Unit V, the minimum thickness areas (also ~E-W aligned) coincide with the location of the horsts, whereas the thicker areas are found within the grabens (Figures 10a and 10b). We refer to Unit V as the synextensional sedimentary sequence in the Coral Patch Ridge and Seine Abyssal Plain areas. Above this unit and following a concordant configuration, the isochore map of Units IV-II shows fairly constant low thickness (0.2–0.4 s TWTT or 200–350 m thick) in agreement with a period of tectonic quiescence in the region (Figures 8, 9, 10c, and 11). We refer to the Units IV-II as the postextensional sedimentary sequence in the Coral Patch Ridge and Seine Abyssal Plain domains. In contrast, in the Horseshoe Abyssal Plain Units IV-II are thicker (<2 s TWTT) than in the southern area and show significant lateral variations in thickness (Figure 10c). These observations may indicate the generation of space to accommodate sediments due to tectonic activity (i.e., the early opening of the North Atlantic). In this domain we refer to this succession as the synextensional sedimentary sequence.

[37] After the Lower Oligocene plate reorganization (i.e., chron C13n), convergent motion between Africa and Eurasia was accommodated along the southern margin of Iberia. Since then, Iberia has remained fixed relative to Eurasia and the current plate boundary between North Africa and Iberia was established [*Schettino and Turco*, 2009]. During this phase took place the sedimentation of Unit I (Upper Oligocene to present day), which consists mainly of pelagic sediments. The change from terrigenous to pelagic sedimentation took place following a post-Early Eocene to pre-Late Oligocene uplift and faulting period during which the topographic hills were uplifted [*Hayes et al*., 1972]. The isochore map of Unit I shows a minimum thickness in the uplifted structural highs of the Coral Patch Ridge and Seine Hills, whereas the depocenters are northwest from it (Figure 10d). In the Seine Abyssal Plain, growth-strata configuration of the subunits is identified (Figures 5, 8, 9, and 11) suggesting that sedimentation of Unit I has been synchronous to the activity of the uplifting structures (NCP, SCP, and SH). Thus, we refer to Unit I as the syncompressional sedimentary sequence.

[38] Between the predominantly terrigenous sedimentation of Unit II (Lower Eocene) and subunit Id (Upper Oligocene) dominated by pelagic sediments, there is a significant unconformity corresponding to a regional sedimentary hiatus (Figures 4, 5, 8, 9, and 11). Subunit Id is not identified in the Horseshoe Abyssal Plain probably because of erosion during the emplacement of subunit Ic (HGU) in the Upper Miocene (Tortonian) [e.g., *Torelli et al*., 1997] (Figures 7, 8, and 11). Within the HGU, we identified few subhorizontal reflectors, suggesting mass transport deposition during several episodes (Figure 7). The lack of interdigitations between the edges of this subunit and surrounding sediments could be explained either by sedimentation in a very short period of time or by a successive deposition in increasingly smaller areas within the HGU [*Iribarren et al*., 2007] (Figures 7 and 11). All the subunits of Unit I vary considerably in thickness, attaining maximum thickness in the abyssal plains and pinching out into a wedge toward the top of the Coral Patch Ridge. In the isochore map of Unit I is observed that the LS separates two depocenters, suggesting that the activity of this fault may have influenced the sediment distribution of this unit.

[39] As for the structural pattern of the region, flat-ramp-flat geometries of large thrusts dominate in the Coral Patch Ridge and Seine Abyssal Plain areas (Figures 8, 9, and 11). In the shallow part of the Seine Hills, structural wedges developed at the tips of the upper flats with associated back-thrusts. In the MCS profiles, these structures appear to cut and displace the synextensional and postextensional sedimentary sequences, and in some cases, the syncompressional unit (Figure 11). In the Coral Patch Ridge domain, the shallow part of the SCP fault is imaged displacing both sedimentary sequences up to the seafloor, whereas the NCP fault corresponds to a blind-thrust. The main thrusts (NCP, SCP, SH2, SH3, SH4, and SH6) probably root in lower flats that are outside the MCS acquisition window. According to the accepted fault-related folding theory [e.g., *Shaw*

et al., 2005], these thrusts are interpreted as propagating from a common deep detachment layer, which could be located either at the base of the crust (Moho discontinuity) in agreement with *Sartori et al*. [1994] and *Zitellini et al*. [2009] or at the base of the serpentinized area in the uppermost mantle [*Martínez-Loriente et al*., 2011]. On the basis of the wide-angle seismic profile P1 crossing this region, the depth of the Moho is about 7–8 km depth below the seafloor and the maximum depth of the serpentinized area in the upper mantle is between 12 and 13 km depth below the seafloor [*Martínez-Loriente et al*., 2011] (Figure 11). In the Coral Patch Ridge and Seine Abyssal Plain domains, secondary thrusts and transpressive strike-slip faults cut and offset the basement, the synextensional and postextensional sequences and fold the syncompressional units. These structures are interpreted as rooting in a common shallow level located at the uppermost oceanic crust (∼2.5–4.5 km depth below the seafloor). In the eastern part of the Horseshoe Abyssal Plain, large strike-slips faults such as LS displace the basement and all the sedimentary sequences above. In plain view, they result in the elongated highs deforming the seabed of the Horseshoe Abyssal Plain (Figure 11).

6.2. Synthesis of Active Faults in the Coral Patch Ridge Area

[40] The joint interpretation of the multiscale seismic profiles and acoustic data is summarized on a structural map of the external part of the Gulf of Cadiz, focusing on the active faults (Figure 12). According to the regional strain ellipse, with a direction of maximum principal stress ($\sigma 1$) that follows the NW-SE trending Eurasia-Africa plate convergence, compressive structures trend NE-SW and right-lateral and left-lateral strike-slip faults trend WNW-ESE and NNE-SSW, respectively (Figure 12).

[41] The largest NE-SW trending compressive structures correspond to the Coral Patch Ridge and Seine Hills (Figures 11 and 12). In the Coral Patch Ridge, both active thrusts (NCP and SCP) show segmented fault traces and are offset by WNW-ESE trending dextral faults (Figures 8 and 12), indicating that the activity of these structures started later than in the reverse faults. This is in agreement with the strain patterns and timing of deformation obtained from analogue modeling of fault systems from the external part of the Gulf of Cadiz [e.g., *Rosas et al*., 2009, 2012]. In the NCP fault, the vertical offset decreases toward the surface, whereas in the SCP fault it remains constant, suggesting that it corresponds to a very recent structure. In the Seine Abyssal Plain, we highlight the presence of the Seine Hills, a series of NE-SW trending active-blind thrusts. When the strike of these faults changes to ∼E-W, such as in the SH1, our data reveal transpressive behavior (Figure 12). The vertical offset in the Seine Hills faults is fairly constant over time, as in the SCP fault. This, together with the fact that the main activity of the Gorringe Bank thrust concentrated between the Late Oligocene and Middle Miocene [e.g., *Jiménez-Munt et al*., 2010] suggests a possible southward migration of deformation.

[42] The WNW-ESE dextral strike-slip faults are mainly concentrated in the Horseshoe Abyssal Plain although a large number of them were mapped across the Coral Patch Ridge and the northern part of the Seine Abyssal Plain (Figure 12). These newly mapped strike-slip faults have the same orientation, behavior and timing of deformation as the SFZ defined by *Zitellini et al*. [2009]. The strike-slip faults are concentrated in a WNW-ESE trending band that runs from the Gorringe Bank to the Moroccan slope. Their orientation, behavior and location suggest that they probably correspond to a reactivation of inherited structures from a Jurassic transfer zone, a plate boundary located between Iberia and Morocco referred as the Gibraltar Fault [e.g., *Schettino and Turco*, 2009]. In contrast to what has been previously proposed [e.g., *Sartori et al*., 1994; *Zitellini et al*., 2009], the NE-SW trending thrusts located south of the SFZ are active (Figures 11 and 12). Their orientation and location suggest that these structures probably grew through weakened zones by fracturing due to the opening of the north-east segment of the Jurassic Central Atlantic rifting [e.g., *Schettino and Turco*, 2009].

[43] There are few cases in the world where processes of active deformation under compressional stresses affect old oceanic lithosphere, as in the external Gulf of Cadiz. One of the best-documented examples is in the Central Indian Ocean Basin, where active WSW-ENE reverse faults and N-S fracture zones involving Mesozoic oceanic crust have been recognized [e.g., *Weissel et al*., 1980; *Bull and Scrutton*, 1990, 1992; *Gordon et al*., 1990]. These structures are interpreted as reactivated normal faults and fracture zones generated at a spreading centre [e.g., *Bull and Scrutton*, 1990, 1992], and are seismically active [e.g., *Bergman and Solomon*, 1985].

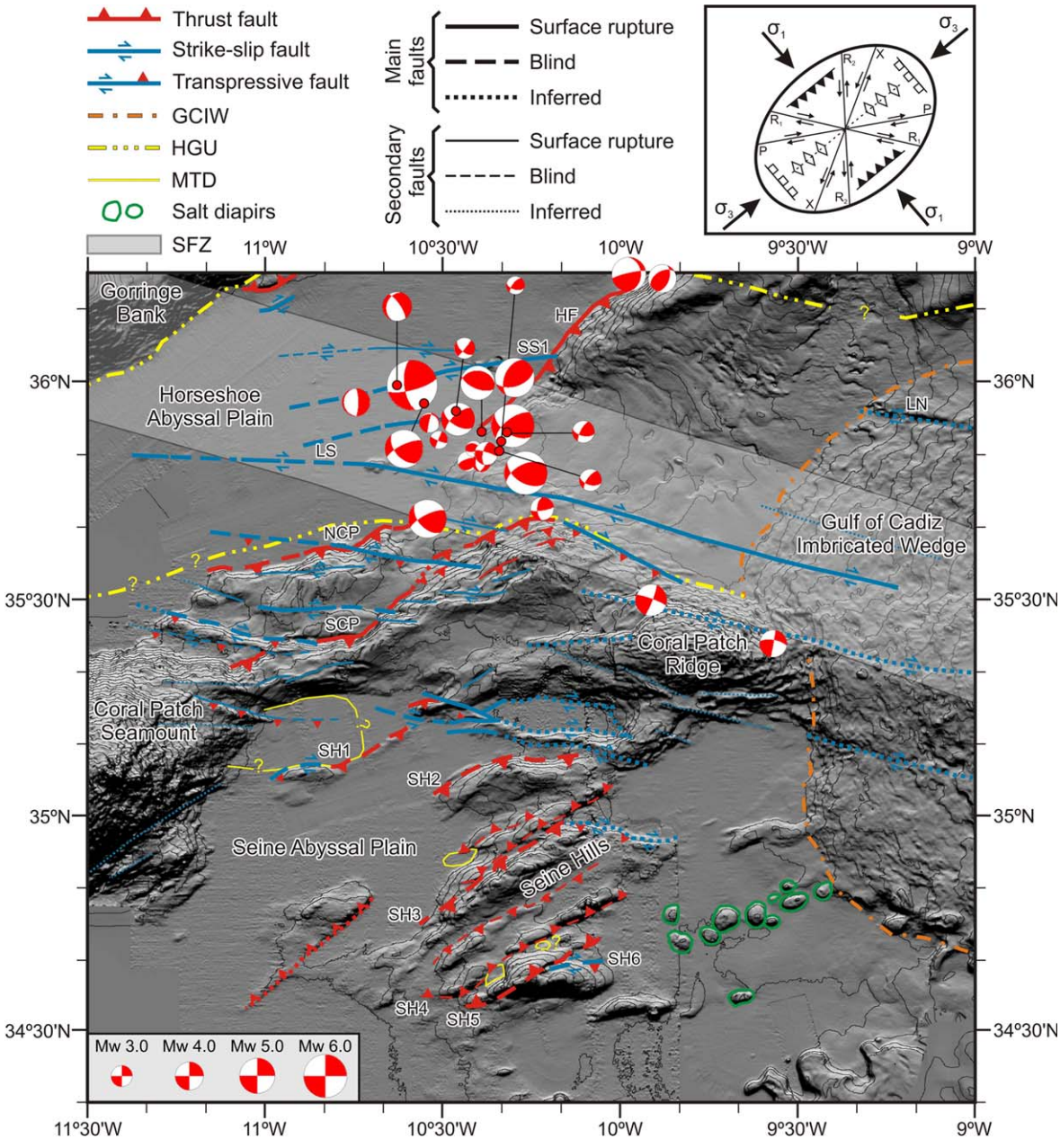

Figure 12. Map of the active faults identified in the study area. Focal mechanisms of recent earthquakes of magnitude $3.0 < Mw > 6.0$ are also included [*Stich et al*., 2005, 2010*; Geissler et al*., 2010]. The SWIM Fault Zone (SFZ) [*Zitellini et al*., 2009] is depicted as a transparent gray band. The Lineament North (LN) and Lineament South (LS) are in agreement with *Bartolome et al*. [2012]. GCIW: Gulf of Cadiz Imbricated Wedge; HGU: Horseshoe Gravitational Unit; MTD: Mass Transport Deposit; HF: Horseshoe Fault; NCP: North Coral Patch Ridge Fault; SCP: South Coral Patch Ridge Fault; SH: Seine Hills faults; SS1: Strike-slip Fault 1. Inset: Strain ellipse with a NW-SE direction of maximum principal stress (σ1) parallel to the vector of the Eurasia-Africa plate convergence in SW Iberia, explaining the occurrence and trend of the different tectonic structures recognized in the area.

[44] The seismicity recorded in the study area is mainly concentrated along the strike-slip faults of the Horseshoe Abyssal Plain (Figures 1 and 12). Moment tensor inversions of these earthquakes, which nucleated between 45 and 55 km deep, reveal WNW-ESE trending nodal planes with a reverse and right-lateral slip at shallow to intermediate depths (8–55 km) [*Geissler et al*.,

Table 1. Main Seismic Parameters of the Large Active Faults in the Studied Area[a]

Fault Name	Length (km)	Dip (°)	Rake (°)	Average Strike (°)		Seismogenic Depth (km)[a]		Width (km)		Area (km^2)		Seismic moment (M_0)		Moment magnitude (M_w)	
				W seg.	E seg.	Min.	Max.	Min.	Max.	Min.	Max.	Min.	Max.	Min.	Max.
SS1	68 ± 5	85 ± 5	180	080		45	55	45.2 ± 0.3	55.2 ± 0.4	3072 ± 203	3754 ± 248	$(4.4 \pm 0.61) \times 10^{20}$	$(5.4 \pm 0.75) \times 10^{20}$	7.8 ± 0.1	7.8 ± 0.1
LS	180 ± 5	85 ± 5	180	095	105	45	55	45.2 ± 0.3	55.2 ± 0.4	8131 ± 164	9938 ± 201	$(3.1 \pm 0.15) \times 10^{21}$	$(3.8 \pm 0.18) \times 10^{21}$	8.3 ± 0.1	8.4 ± 0.1
NCPF	65 ± 5	30 ± 5	90	050	080	5.7	11	11.4 ± 1.8	22.0 ± 3.4	741 ± 57	1430 ± 110	$(6.7 \pm 0.06) \times 10^{19}$	$(1.3 \pm 0.01) \times 10^{20}$	7.2 ± 0.1	7.4 ± 0.1
SCPF	83 ± 5	30 ± 5	90	078	053	7.2	12.5	14.4 ± 2.2	25.0 ± 3.9	1195 ± 112	2075 ± 195	$(1.4 \pm 0.04) \times 10^{20}$	$(2.4 \pm 0.08) \times 10^{20}$	7.4 ± 0.1	7.6 ± 0.1
SH3	45 ± 5	30 ± 5	90	055		7.5	12.7	15.0 ± 2.3	25.4 ± 4.0	675 ± 28	1143 ± 47	$(4.3 \pm 0.30) \times 10^{19}$	$(7.2 \pm 0.51) \times 10^{19}$	7.1 ± 0.1	7.2 ± 0.1

[a]Seismogenic depth refers to kilometers below the seafloor.

2010]. The nucleation of earthquakes at these depths suggests that they occur within the upper mantle [*Stich et al.*, 2010; *Bartolome et al.*, 2012].

6.3. Seismic Potential of the Largest Faults: Implications for Earthquake and Tsunami Hazard Assessment Models

[45] To evaluate the seismic potential of the largest strike-slip and thrust faults, we measured the segment length, dip and rake, and we estimated minimum and maximum potential seismogenic depths, obtaining the correspondent maximum surface ruptures (Table 1). As global-scale empirical magnitude-area and magnitude-length relationships, such as those proposed by *Wells and Coppersmith* [1994], exclude earthquakes occurring within oceanic lithosphere, we estimated the maximum earthquake magnitudes (M_w) using the seismic moment (M_0), where $M_0 = \mu \cdot S \cdot D$; μ is the shear modulus (rigidity) of faulted rocks; S is the fault surface rupture; and D is the average displacement along the fault. We considered an average rigidity of $\mu \approx 60$ GPa for the upper mantle and of $\mu \approx 40$ GPa for the oceanic crust [*Stich et al.*, 2007]. Regarding the slip-to-length ratio, due to the lack of seismic information in the area of this study, we considered the value of $3.5 \cdot 10^{-5}$ proposed for the Gulf of Cadiz region [e.g., *Stich et al.*, 2007]. The moment magnitudes (M_w) were calculated following the relationship between the seismic moment and the moment magnitude as $M_w = 2/3 \cdot \log_{10}(M_0) - 6.0$ [*Kanamori*, 1977].

[46] To calculate the M_w values for both families of faults we consider two different scenarios depending on the seismogenic depths assumed (Table 1). In the case of the strike-slip faults we know that nucleation of earthquakes occurred between 45 and 55 km depth [*Stich et al.*, 2005, 2010; *Geissler et al.*, 2010]. Thus, assuming an average dip of 85° ± 5° and the measured length of each fault with an error of ±5 km due to the bathymetric resolution, the M_w values obtained for the LS vary between 8.3 ± 0.1 and 8.4 ± 0.1, whereas for the SS1 is 7.8 ± 0.1 in both scenarios (Figure 13a, Table 1). In the case of thrust faults, it is not possible to estimate their maximum seismogenic depths. On the basis of our structural interpretation, we also assume two possible scenarios: either the thrusts are rooted in the Moho, at about 8 km, or they root below the serpentinized area in the uppermost mantle, at 13 km below the seafloor (Figure 11). Thus, considering an average

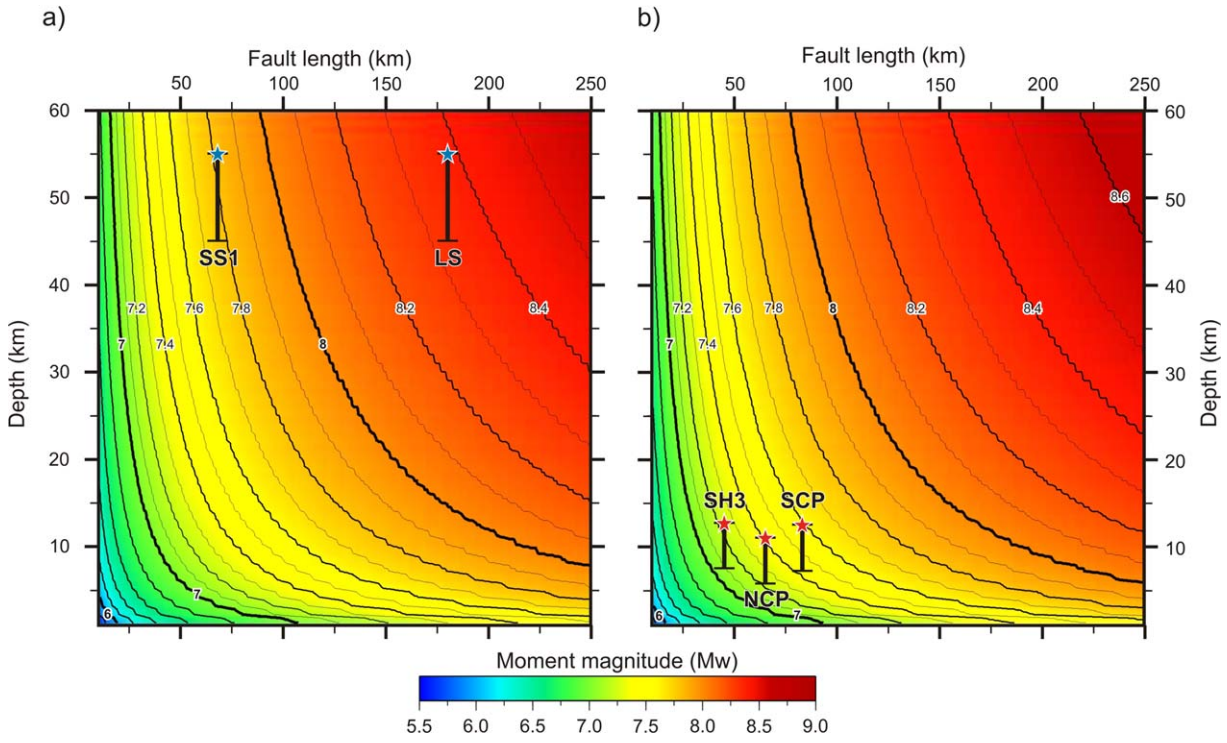

Figure 13. Calculated potential earthquake magnitude (*Mw*) for the largest structures recognized in the area: (a) strike-slip faults (LS and SS1) and (b) thrust faults (NCP, SCP and SH3), as a function of fault length and seismogenic depth. Rigidity (μ), slip-to-length ratio and depth (D) were assumed as constant. The values used for strike-slip faults are $\mu \approx 60$ GPa, slip-to-length ratio of $3.5 \cdot 10^{-5}$ and a fault dip of 85°; and for thrust faults are $\mu \approx 40$ GPa, slip-to-length ratio of $3.5 \cdot 10^{-5}$ and a fault dip of 30°. Bars correspond to the bounds of the *Mw* values obtained for the two scenarios and are presented for each of the structures. Stars locate the maximum M_w values. LS: Lineament South; NCP: North Coral Patch Ridge Fault; SCP: South Coral Patch Ridge Fault; SH3: Seine Hill 3 Fault; SS1: Strike-slip Fault 1. See text for further explanations.

dip of 30° ± 5° and the length of each fault with a measurement error of ±5 km, the estimated M_w values calculated for the NCP vary between 7.2 ± 0.1 and 7.4 ± 0.1, for the SCP range between 7.4 ± 0.1 and 7.6 ± 0.1, and for the SH3 vary between 7.1 ± 0.1 and 7.2 ± 0.1 (Figure 13b and Table 1).

[47] The relatively short period of instrumental and historical earthquake catalogues on which seismic hazard assessment in the Iberian Peninsula is largely based, may not be sufficient when considering high magnitude earthquakes with long recurrence intervals. For instance, on the basis of seismically triggered turbidites found in the deep basins, the regional recurrence interval of Great earthquakes ($Mw \geq 8.0$) in the SW Iberian Margin during the Holocene is approximately 1800 years [*Gràcia et al.*, 2010]. If we consider the maximum earthquake magnitude obtained for the largest faults in the study area (M_w 7.2–8.4), the evaluated structures might be capable of generating large earthquakes, and given their oceanic location (150 km offshore Portugal), they may represent a geohazard for the surrounding coastal areas. The strike-slip faults probably cannot generate devastating tsunamis by themselves despite the possibility of a vertical slip component and a related seafloor displacement along the LS and SS1. However, large magnitude earthquakes may trigger associated slope failures, such as the North Gorringe Avalanche [*Lo Iacono et al.*, 2012], increasing the overall tsunami risk. All the structures studied in the present work should therefore be considered in future seismic and tsunami hazard assessment models for the southwest Iberia and north Africa.

7. Conclusions

[48] The combined interpretation of high-resolution SWIM 2006 MCS reflection profiles

together with swath-bathymetry, subbottom profiles and sediment cores yield new insights into the tectonic architecture and crustal structure of the Coral Patch Ridge area and surrounding abyssal plains. The geometry of the seismostratigraphic units allowed us to characterize successive deformation phases in the outer part of the Gulf of Cadiz and to distinguish the synextensional, postextensional, and syncompressional sedimentary sequences in each domain.

[49] NE-SW trending thrusts (NCP, SCP, and SH1-SH6) and WNW-ESE trending subvertical dextral strike-slip faults (e.g., LS and SS1) occur in the old oceanic lithosphere of the Horseshoe Abyssal Plain, Coral Patch Ridge and Seine Abyssal Plain, and are consistent with the NW-SE regional shortening axis between Eurasia and Africa. These structures cut, fold or show growth-strata configuration in the most recent sedimentary units of Holocene age, indicating that they are active. The major thrust faults in the Coral Patch Ridge and Seine Abyssal Plain probably propagated from the same detachment level located at the Moho (~7–8 km depth below the seafloor), although they could eventually root at greater depths below the serpentinized area in the uppermost mantle at ~12–13 km below the seafloor (Figure 11). Secondary structures probably also propagated from a shallower detachment level in the upper part of the oceanic crust (between 2.5 and 4.5 km depth below the seafloor). Furthermore, the NE-SW trending thrusts located south of the SFZ probably grew through weakened zones by fracturing due to the opening of the NE segment of the Jurassic Central Atlantic rifting, whereas the WNW-ESE trending strike-slip faults concentrated in the Horseshoe Abyssal Plain may correspond to a reactivation of inherited structures from a Jurassic transfer zone located across the Straits of Gibraltar. The strike-slip faults are seismogenically active with earthquakes nucleating in the upper mantle (>50 km). The SW Iberian Margin may be considered an analogous of the Central Indian Ocean Basin, as in both regions similar active deformation structures involving Mesozoic oceanic lithosphere have been recognized.

[50] As for the earthquake and tsunami hazard assessment, the strike-slip faults represent one of the largest clusters of seismicity in the Gulf of Cadiz, whereas a maximum earthquake of $M_w > 8$ could be generated by the LS. South of the SFZ, despite the low seismic activity recorded in the area, our data suggest that the thrusts are active and potential sources of large magnitude ($M_w > 7$) seismic events and associated tsunamis. Seismic and tsunami hazard in the South Iberian and North African coasts would significantly increase if offshore active structures such as those identified in the Coral Patch Ridge region were considered.

Acknowledgments

[51] The authors acknowledge the support of the Spanish Ministry of Science and Innovation (MICINN) through National Projects EVENT (CGL2006–12861-C02-02) and SHAKE (CGL2011–30005-C02-02); the European Transnational Access SALVADORE program of the EU (RITA-CT-2004–505322), the ESF EuroMargins SWIM project (01-LEG-EMA09F and REN2002–11234E-MAR), the EU program "Global Change and Ecosystems" contract n. 037110 (NEAREST), the ESF TopoEurope TOPOMED project (CGL2008–03474-E/BTE), and the SWIMGLO project (PTDC/MAR/100522/2008). We also acknowledge funding from the MICINN through the "Ramon y Cajal" program (R. Bartolome) and from the CSIC through a JAE Pre-Doc fellowship (S. Martínez-Loriente). Grateful thanks are also due to the captain, crew, scientific and UTM-CSIC technical staff on board the R/V Hespérides, during the SWIM 2006 cruise. We also thank collaboration from R. B. Wynn and D. G. Masson (NOC, UK) for allowing us sampling and dating core JC27-20 from the Seine Abyssal Plain. We thank G-cubed editor Thorsten Becker (USC, USA) and three anonymous reviewers for helpful suggestions and constructive comments. This work was carried out within the Grups de Recerca de la Generalitat de Catalunya B-CSI (2009 SGR 146).

References

Allmendinger, R. W. (1998), Inverse and forward numerical modelling of trishear fault-propagation folds, *Tectonics*, *17*, 640–656.

Argus, D. F., R. G. Gordon, C. DeMets, and S. Stein (1989), Closure of the Africa-Eurasia-North America plate motion circuit and tectonics of the Gloria fault, *J. Geophys. Res.*, *94*, 5585–5602.

Baptista, M. A., and J. M. Miranda (2009), Revision of the Portuguese catalogue of tsunamis, *Nat. Hazards Earth Syst. Sci.*, *9*, 25–42.

Baptista, M. A., P. M. Miranda, J. M. Miranda, and L. M. Victor (1998), Constrains on the source of the 1755 Lisbon Tsunami inferred from numerical modelling of historical data, *J. Geodyn.*, *25*, 159–174.

Baptista, M. A., J. M. Miranda, F. Chierici, and N. Zitellini (2003), New study of the 1755 earthquake source based on multichannel seismic survey data and tsunami modeling, *Nat. Hazards Earth Syst. Sci.*, *3*, 333–340.

Bartolome, R., E. Gràcia, D. Stich, S. Martinez-Loriente, D. Klaeschen, F. L. Mancilla, C. Lo Iacono, J. J. Dañobeitia, and N. Zitellini (2012), Evidence for active strike-slip faulting along the Eurasia-Africa convergence zone: Implications for seismic hazard in the SW Iberian Margin, *Geology*, *40*(6), 495–498, doi:10.1130/G33107.1.

Bergman, A., and C. Solomon (1985), Earthquake source mechanisms from body wave inversion and intra-plate tectonics in the Northern Indian Ocean, *Phys. Earth Planet. Inter.*, *40*, 1–23.

Buforn, E., M. Bezzeghoud, A. Udias, and C. Pro (2004), Seismic sources on the Iberia-African plate boundary and their tectonic implications, *Pure Appl. Geophys.*, *161*, 623–646, doi:10.1007/s00024-003-2466-1.

Bull, J. M., and R. A. Scrutton (1990), Fault reactivation in the Central Indian Ocean Basin and the rheology of the oceanic lithosphere, *Nature*, *344*, 855–858.

Bull, J. M., and R. A. Scrutton (1992), Seismic reflection images of intraplate deformation, central Indian Ocean, and their tectonic significance, *J. Geol. Soc.*, *149*, 955–966, doi:10.1144/gsjgs.149.6.0955.

Contrucci, I., F. Klingelhöfer, J. Perrot, R. Bartolomé, M. A. Gutscher, M. Sahabi, J. Malod, and J. P. Rehault, (2004), The crustal structure of the NW-Moroccan Continental Margin for wide-angle and reflection seismic data, *Geophys. J. Int.*, *159*(1), 117–128, doi:10.1111/j.1365-246X.2004.02391.x.

DeMets, C., R. G. Gordon, and D. F. Argus (2010), Geologically current plate motions, *Geophys. J. Int.*, *181*, 1–80, doi:10.1111/j.1365-246X.2009.04491.x.

Erslev, E. A. (1991), Trishear fault-propagation folding, *Geology*, *19*(6), 617–620.

Fukao, Y. (1973), Thrust faulting at a Lithospheric plate boundary, the portugal earthquake of 1969, *Earth Planet. Sci. Lett.*, *18*, 205–216.

Geissler, W. H., et al. (2010), Focal mechanisms for subcrustal earthquakes in the Gulf of Cadiz from dense OBS deployment, *Geophys. Res. Lett.*, *37*, L18309, doi:10.1029/2010GL044289.

Gordon, R. G., C. DeMets, and D. F. Argus (1990), Kinematic constraints on distributed lithospheric deformation in the equatorial Indian Ocean from present motion between the Australian and Indian plates, *Tectonics*, *9*, 409–423.

Gràcia, E., J. J. Dañobeitia, J. Vergés, and PARSIFAL Team (2003a), Mapping active faults offshore Portugal (36°N–38°N): Implications for seismic hazard assessment along the southwest Iberian margin, *Geology*, *31*, 83–86.

Gràcia, E., J. J. Danobeitia, J. Verges, and R. Bartolome (2003b), Crustal architecture and tectonic evolution of the Gulf of Cadiz (SW Iberian margin) at the convergence of the Eurasian and African plates, *Tectonics*, *22*(4), 1033, doi:10.1029/2001TC901045.

Gràcia, E., A. Vizcaino, C. Escutia, A. Asioli, A. Rodés, R. Pallàs, J. Garcia Orellana, S. Lebreiro, and C. Goldfinger (2010), Holocene earthquake record offshore Portugal (SW Iberia): Testing turbidite paleoseismology in a slow-convergence margin, *Quat. Sci. Rev.*, *29*, 1156–1172.

Gutscher, M. A., J. Malod, J. P. Rehault, I. Contrucci, F. Klingelhoefer, L. Mendes-Victor, and W. Spakman (2002), Evidence for active subduction beneath Gibraltar, *Geology*, *30*, 1071–1074.

Hayes, D. E., et al. (1972), *Initial Reports of the Deep Sea Drilling Project*, Leg 14, pp. 15–48, U.S. Gov. Print. Off., Washington, D. C.

Hayward, N., A. B. Watts, G. K. Westbrook, and J. S. Collier (1999), A seismic reflection and GLORIA study of compressional deformation in the Gorringe Bank region, eastern north atlantic, *Geophys. J. Int.*, *138*(3), 831–850.

I.G.N. (2012). Boletín de sismos próximos, report, Instituto Geográfico Nacional, Madrid (Spain), http://www.ign.es/ign/layoutIn/sismoFormularioCatalogo.do.

Iribarren, L., J. Vergés, F. Camurri, J. Fullea, and M. Fernàndez (2007), The structure of the Atlantic-Mediterranean transition zone from the Alboran Sea to the Horseshoe Abyssal Plain (Iberia–Africa plate boundary), *Mar. Geol.*, *243*, 97–119.

Jiménez-Munt, I., M. Fernàndez, J. Vergés, J. C. Afonso, D. Garcia-Castellanos, and J. Fullea (2010), Lithospheric structure of the Gorringe Bank: Insights into its origin and tectonic evolution, *Tectonics*, *29*, TC5019, doi:10.1029/2009TC002458.

Johnston, A. C. (1996), Seismic moment assessment of earthquakes in stable continental regions-III New Madrid 1811–1812, Charleston 1886 and Lisbon 1755, *Geophys. J. Int.*, *126*(2), 314–344.

Kanamori, H. (1977), The energy release in great earthquakes, *J. Geophys. Res.*, *82*, 2981–2987, doi:10.1029/JB082i020p02981.

Lebreiro, S. M., I. N. McCave, and P. P. E. Weaver (1997), Late quaternary turbidite emplacement on the Horseshoe Abyssal Plain (Iberian Margin), *J. Sediment. Res.*, *67*(5), 856–870.

Lo Iacono, C., et al. (2012), Large, deep water slope failures: Implications for landslide-generated tsunamis, *Geology*, *40*(10), 931–934.

Martínez-Loriente, S., V. Sallarès, A. Gailler, R. Bartolomé, E. Gràcia, M. A. Gutscher, and J. Diaz (2011), Crustal nature and seismic structure of the geological provinces offshore the SW Iberia: Highlights of the NEAREST-SEIS wide-angle seismic survey, Abstract T43E-2409 presented at 2011 Fall Meeting, AGU, San Francisco, Calif., 5-9 Dec.

Martínez-Solares, J. M. (2003), Historical seismicity of the Iberian Peninsula, *Fis. Tierra*, *15*, 13–28.

McBarnet, A. (2000), How GXT caught the pre-stack depth imaging wave, *First Break*, *18*(3), 109–111.

Medialdea, T., R. Vegas, L. Somoza, J. T. Vázquez, A. Maldonado, V. Díaz-del-Río, A. Maestro, D. Córdoba, and M. C. Fernández-Puga (2004), Structure and evolution of the ''Olistostrome'' complex of the Gibraltar Arc in the Gulf of Cadiz (eastern Central Atlantic): Evidence from two long seismic cross-sections, *Mar. Geol.*, *209*(1-4), 173–198.

Medwedeff, D. A. (1989), Growth fault-bend folding at southeast Lost Hills, San Joaquin Valley, California, *AAPG Bull.*, *73*, 54–67.

Mezcua, J., J. Rueda, and R. M. Blanco (2004), Reevaluation of historic earthquakes in Spain, *Seismol. Res. Lett.*, *75*, 75–81.

Nocquet, J. M., and E. Calais (2004), Geodetic measurements of crustal deformation in the Western Mediterranean and Europe, *Pure Appl. Geophys.*, *161*, 661–681.

Purdy, G. M. (1975), The Eastern end of the Azores-Gibraltar plate boundary, *Geophys. J. R. Astron. Soc.*, *43*, 123–150.

Rosas, F. M., J. C. Duarte, P. Terrinha, V. Valadares, and L. Matias (2009), Morphotectonic characterization of major bathymetric lineaments in Gulf of Cadiz (Africa – Iberia plate boundary): Insights from analogue modeling experiments, *Mar. Geol.*, *261*(1-4), 33–47, doi:10.1016/j.margeo.2008.08.002.

Rosas, F. M., J. C. Duarte, M.C. Neves, P. Terrinha, S. Silva, L. Matias, E. Gràcia, and R. Bartolome (2012), Thrust-wrench interference between major active faults in the Gulf of Cadiz (Africa-Eurasia plate boundary, offshore SW Iberia): Tectonic implications from coupled analog and numerical modeling, *Tectonophysics*, *548-549*, 1–21, doi:10.1016/j.tecto.2012.04.013.

Rovere, M., C. R. Ranero, R. Sartori, L. Torelli, and N. Zitellini (2004), Seismic images and magnetic signature of Late

Jurasic to Early Cretaceous Africa-Eurasia plate boundary off SW Iberia, *Geophys. J. Int.*, *158*, 554–568.

Ryan, W. B. R., et al. (1973), Initial Reports of the Deep Sea Drilling Project, Volume XIII, Washington (U.S. Government Printing Office), pp. 19–41.

Sallarès, V., A. Gailler, M. A. Gutscher, D. Graindorge, R. Bartolomé, E. Gràcia, J. Díaz, J. J. Dañobeitia, and N. Zitellini (2011), Seismic evidence for the presence of Jurassic oceanic crust in the central Gulf of Cadiz (SW Iberia margin), *Earth Planet. Sci. Lett.*, *311*, 112–123, doi:10.1016/j.epsl.2011.09.003.

Sallarès, V., S. Martínez-Loriente, M. Prada, E. Gràcia, C. R. Ranero, M. A. Gutscher, R. Bartolome, A. Gailler, J. J. Dañobeitia, and N. Zitellini (2013), Seismic evidence of exhumed mantle rock basement at the Gorringe Bank and the adjacent Horseshoe and Tagus abyssal plains (SW Iberia), *Earth Planet. Sci. Lett.*, *365*, 120–131, doi:10.1016/j.epsl.2013.01.021.

Sartori, R., L. Torelli, N. Zitellini, D. Peis, and E. Lodolo (1994), Eastern segment of the Azores-Gibraltar line (central-eastern Atlantic): An oceanic plate boundary with diffuse compressional deformation, *Geology*, *22*, 555–558.

Schettino, A., and E. Turco (2009), Breakup of Pangea and plate kinematics of the central Atlantic and Atlas regions, *Geophys. J. Int.*, *178*, 1078–1097.

Shaw, J. H., C. Connors, and J. Suppe (Eds.) (2005), Seismic Interpretation of Contractional Fault-Related Folds, An AAPG Seismic Atlas: AAPG Studies in Geology, vol. 53, American Association of Petroleum Geologists, Tulsa, Oklahoma, U.S.A. 156 pp.

Stich, D., F. Mancilla, and J. Morales (2005), Crust mantle coupling in the Gulf of Cadiz (SW Iberia), *Geophys. Res. Lett.*, *32*, L13306, doi:10.1029/2005GL023098.

Stich, D., F. Mancilla, S. Pondrelli, and J. Morales (2007), Source analysis of the February 12th 2007, Mw 6.0., Horseshoe earthquake: Implications for the 1755 Lisbon earthquake, *Geophys. Res. Lett.*, *34*, L11208, doi:10.1029/2007GL030012.

Stich, D., R. Martin, and J. Morales (2010), Moment tensor inversion for Iberia-Maghreb earthquakes 2005–2008, *Tectonophysics*, *483*, 390–398, doi:10.1016/j.tecto.2009.11.006.

Srivastava, S. P., H. Schouten, W. R. Roest, K. D. Klitgord, L. C. Kovacs, J. Verhoef, and R. Macnab (1990), Iberian plate kinematics: A jumping plate boundary between Eurasia and Africa, *Nature*, *344*, 756–759.

Suppe, J. (1983), Geometry and kinematics of fault-bend folding, *Am. J. Sci.*, *283*, 684–721.

Suppe, J., C. Connors, and Y. Zhang (2004), Shear fault-bend folding, in *Thrust Tectonics and Hydrocarbon Systems*: AAPG Memoir, 82, edited by K. R. McClay, pp. 303–323.

Terrinha, P., et al. (2003), Tsunamigenic-seismogenic structures, neotectonics, sedimentary processes and slope instability on the southwest Portuguese Margin, *Mar. Geol.*, *195*(1-4), 55–73.

Terrinha, P., et al. (2009), Morphotectonics and strain partitioning at the Iberia–Africa plate boundary from multibeam and seismic reflection data, *Mar. Geol.*, *267*, 156–174.

Torelli, L., R. Sartori, and N. Zitellini (1997), The giant chaotic body in the Atlantic Ocean off Gibraltar: New results from a deep seismic reflection survey, *Mar. Pet. Geol.*, *14*, 125–138.

Tortella, D., M. Torne, and A. Perez-Estaun (1997), Geodynamic evolution of the eastern segment of the Azores–Gibraltar Zone: The Gorringe Bank and Gulf of Cadiz region, *Mar. Geophys. Res.*, *19*, 211–230.

Tucholke, B. E., D. S. Sawyer, and J. C. Sibuet (2007), Breakup of the Newfoundland-Iberia Rift, in *Imaging, Mapping, and Modelling Continental Lithosphere Extension and Breakup*, vol. 282, edited by G. D. Karner, G. Manatschal, and L. M. Pinheiro, pp. 9–46, Geological Society, London, Special Publications.

Weissel, J. K., R. N. Anderson, and C. A. Geller (1980), Deformation of the Indo-Australian plate, *Nature*, *287*, 284–291.

Wells, D. L., and K. J. Coppersmith (1994), New empirical relationships among magnitude, rupture length, rupture width, rupture area, and surface displacement, *Bull. Seismol. Soc. Am.*, *84*, 974–1002.

Zitellini, N., L. Mendes Victor, D. Córdoba, J. J. Dañobeitia, R. Nicolich, G. Pellis, A. Ribeiro, R. Sartori, L. Torelli, and BIGSETS Team (2001), Source of the 1755 Lisbon Earthquake and Tsunami Investigated, *EOS Trans. AGU*, *82*, 285–291.

Zitellini, N., M. Rovere, P. Terrinha, F. Chierici, L. Matias, and BIGSETS Team (2004), Neogene through Quaternary tectonic reactivation of SW Iberian Passive Margin, *Pure Appl. Geophys.*, *161*, 565–587.

Zitellini, N., et al. (2009), The quest for the Africa-Eurasia plate boundary west of the Strait of Gibraltar, *Earth Planet. Sci. Lett.*, *280*, 13–50, doi:10.1016/j.epsl.2008.12.005.